Sup.

UNIVERSITY OF CAMBRIDGE
Department of Engineering

# Foundations for Floating Offshore Wind Farms

Division D
Fourth-Year Undergraduate Project

*Author*
Chen Ma (cm707)
Trinity College

*Supervisor*
Professor Gopal Santana Phani Madabhushi

Date: May 24, 2016

I hereby declare that, except where specifically indicated, the work submitted herein is my own original work.

*Signed* Chen Ma *date* May 24, 2016

# Foundations for Floating Offshore Wind Farms - Technical Abstract

*Author*: Chen Ma (cm707) Trinity College *Supervisor*: Professor Gopal Santana Phani Madabhushi

Offshore wind farms represent a promising solution for renewable electricity generation. It is estimated to meet the 14% of the EU's total electricity demand by 2030. There is abundant wind resource in deep waters such as North Sea. To allow an economic development of a wind farm design in deep waters, it is necessary to employ floating systems instead of fixed foundations. However, by the end of 2012, more than 99% of the offshore wind farms are based on fixed foundations. Although the environmental conditions are challenging, there is also a huge market drive to develop wind farms in deep seas. The design and modelling of a deep sea wind farm has become a popular topic in the academic world.

To conclude an efficient design, it is often required to do software simulations first. However, software simulations alone can sometimes be misleading and may result in unexpected behaviours. The aim of this project is, therefore, to use a physical modelling method to enhance the validity of a design.

There are few types of floating systems including ballast stabilised type, tension leg platform type (TLP) and buoyancy stabilised type. It is concluded that the TLP type is the most economical for both development and construction processes. TLP wind turbines usually provide less movement in wind and wave forces than the other two types, and they are relatively easy to be constructed. Therefore, the TLP type has been chosen as the model of the wind farm foundation in this project. The model to be used is not a scaled-down version of a wind farm but a rudimentary TLP model. Although the performance may be different from an actual offshore wind farm, the experimental method should remain similar. Gradual improvements can be made to the model which may eventually represent a scaled model of a TLP wind turbine.

Figure 1 shows the experimental setup of this project. The system is made of a floating box with four tendons attached to the bottom of a shaking table. The whole TLP is situated within a water tank. Frequency of the shaking table, and hence the water in the water tank, can be controlled to simulate ocean waves.

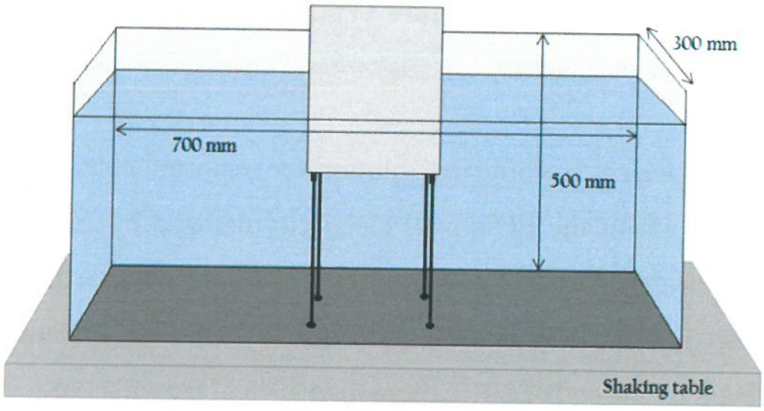


Figure 1 Experimental setup

In the experiments of this project, several performance factors were considered including depth of water displaced by the floating system, weight of the system, tension within the mooring lines and depth of embedment for anchor foundations. By employing sensor technologies and signal processing (MATLAB), it was possible to monitor accelerations of the model and tension of the mooring. This enables the investigation of different parameters and their respective behaviours. Key investigations include the following:

1. Using acceleration and tension data to conclude the natural frequency of the system
2. Comparison of system responses of different model materials and hence different mass
3. Comparison of system responses of different volumes of water displaced
4. Model design for plate anchor foundations and investigation of embedment depth

There are two stages of this project. The first phase was to use fixed mooring to investigate the system responses to different parameters such as volume of water displaced and effect of mass. The second phase will employ a plate anchor foundation system to allow a more realistic situation in offshore environment, and to investigate the depth of embedment.

Main conclusions include:

1. A lighter weight floating system will have a higher acceleration response in the same ocean wave.
2. A smaller volume of water displaced by the floating box will lead to a lower natural frequency.
3. The physical modelling method is valid in designing a TLP wind farm, and improvements can be made gradually to eventually have a scaled model.

Keywords: offshore wind farm, tension leg platform, floating system

**Technical abstract**

**Contents**

# 1. Introduction

## 1.1 Background

According to Arapogianni and Genachte (European Wind Energy Association), Europe's seas and oceans are rich in opportunities and sources in wind generation [1]. It is still a new industry facing lots of challenges, but it is one of the fastest growing maritime sectors. The installed capacity was 5 GW at the end of 2012, and by 2020 this could be as much as 40 GW, meeting 4% of European electricity demand. By 2030, offshore wind capacity may reach 150 GW, meeting 14% of the EU's total electricity consumption. There is a huge demand for development and construction of new offshore wind farms.

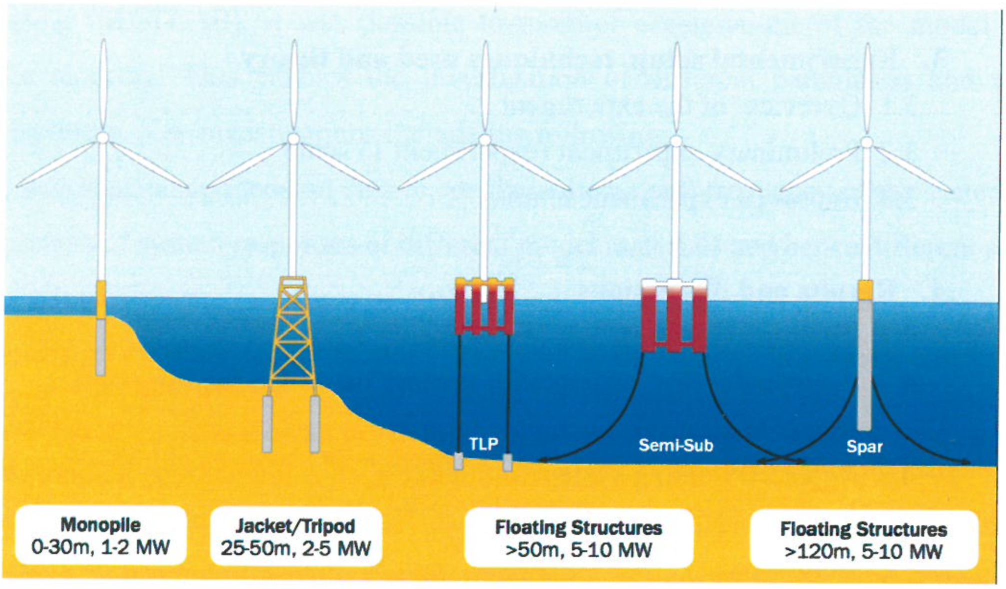


Figure. 1.1.1 Offshore wind farm foundation type, [1]

Figure 1.1.1 shows major types of offshore foundations for different depth of water. The substructure types of offshore wind farms have been dominated by the fixed foundation types namely pile foundations, gravity-based foundations and frame foundations [1]. These types of foundations are typically used for water depths up to 50 m [2]. By the end of 2012, more than 99% of the offshore wind farms connected to grid use fixed substructures.

There is a huge market drive for deep sea wind farms using floating wind turbines (FWTs). In 2012, the average depth of wind farms was only 22 m, and the average distance from shore is 29 km. However, projects are announced with water depth up to 215 m and 200 km away from shore. For deep water, existing technology of FWTs are more suitable and economic. [1]

## 1.2 Motivation

Building an offshore wind farm needs to be particularly cost-effective due to its extremely low profitability in short-term. Early involvement of appropriate modelling methods is necessary to complete an efficient design.

Tension leg platforms (TLP) represents a typical type of floating systems for moderately deep water [3]. The motions of TLPs are expected to have lower structural loading on the turbine. The models used are based on tension leg platform wind turbine (TLPWT) designs. Although TLP designs in oil and gas industry can provide some guidance, significant differences such as requirements for precise positioning exist- for example, TLPWTs are not required to maintain a precise position relative to seabed [4]. A physical model will provide a detailed insight into problems like this.

## 1.3 Objectives

This project seeks to investigate the feasibility of using a physical model to determine the performance metrics of a floating system design. There is little effort in investigating the optimal design of a TLP wind farm, but the purpose of the project is to conclude an effective method of determining several performance parameters that are critical to the design. The primary objectives are as follows:

- Measurement of 1-D accelerations at different parts of the TLP model
- Measurement of tension in one of the four tendons of the TLP model
- Using acceleration and tension data to conclude the natural frequency of the system

- Comparison of system responses of different model materials and hence different mass
- Comparison of system responses of different volumes of water displaced
- Model design for plate anchor foundations and investigation of embedment depth

The TLP model used in this project is not a scaled-down version of a full TLPWT but a rudimentary TLP floating system model. Various experiments will be carried out with this model and test results will be compared to evaluate the performance metrics of a TLP system.

## 2. Literature review

Extensive research has been done to investigate the offshore structures. In this section, literatures in regard to offshore environment, deep water foundation types, analysis method and past physical experiments will be reviewed. This is to establish the need to physically investigate the various performance metrics of offshore foundations.

### 2.1 Offshore environment and environmental forces

According to Chandrasekaran [5], loads acting on offshore structures can be classified into the following categories:

- Permanent loads or dead loads
- Operating loads or live loads
- Other environmental loads including earthquake loads
- Construction and installation loads
- Accidental loads

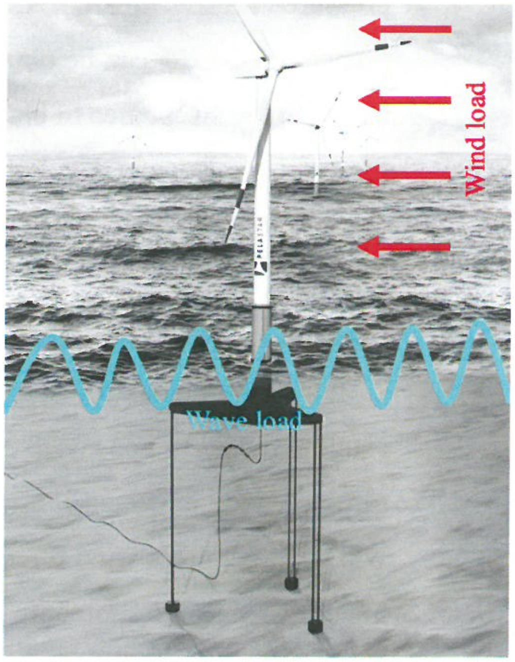

Figure 2.1.1 TLP wind turbine with wind and wave loads, Grzegorz P. Filip

The design for an offshore wind farm will be majorly influenced by the permanent loads and environmental loads including wind and wave forces. In this section, wind and wave forces will be discussed.

A typical wind turbine such as the NREL offshore 5-MW baseline wind turbine has a total mass of 697.46 tonnes with a hub height of 90 m [2]. These huge structures are subject to very high wind load and wave load especially when there is a storm. The design safety factors are usually high. The following sections will illustrate the numerical ways of getting wind force and wave force on a floating structure. This is useful during the early design stage by evaluating the loads with specific design dimensions of the floating structure.

### 2.1.1 Wind force

Wind force on a plate orthogonal to the wind flow direction will have the net wind pressure as given by Eq. 2.1.1:

$$p_W = \frac{1}{2}\rho_a C_W v^2 \qquad (2.1.1)$$

where $\rho_a$ is density of air (1.25 kg/m$^3$ including water splash) and $C_W$ is the wind pressure coefficient. By using a wind tunnel test the $C_W$ can be obtained, and by knowing the swept area of blades, the wind force on the rotor can then be estimated. Typical loads for a 3.5-5 MW turbine, in shallow water can be shown as Figure 2.1.2 [6]. Wind force represents 1-2 MN on the blades for a wind turbine in shallow water. For deep water wind turbines, it is expected that the wind force will be larger. This wind force will generate a huge overturning moment which the foundation needs to accommodate. This overturning moment is the major concern in a design process which need to be carefully considered.

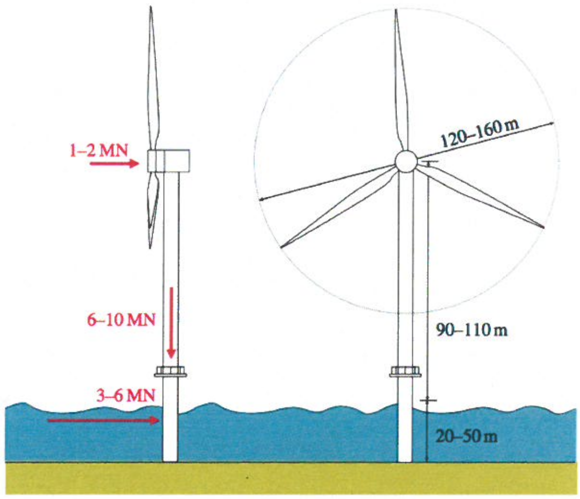

Figure 2.1.2 Loading on an offshore wind turbine in shallow water, Byrne and Houlsby, [6]

### 2.1.2 Wave force

Wave force on the floating structure usually means the forces from sea level waves generated by wind. Airy's wave theory is commonly used to represent a numerical model of an ocean wave (Chandrasekaran [5]). It assumes a sinusoidal wave form (Eq. 2.1.2) of wave height (H), which is small in comparison with the wave length (λ) and water depth (d).

$$\eta(x,t) = \frac{H}{2}\cos(kx - \omega t), \quad where\ k = \frac{2\pi}{\lambda} \qquad (2.1.2)$$

By differentiation and applying boundary conditions, horizontal and vertical velocities and accelerations can be obtained:

$$Horizontal\ velocity\ of\ wave\ particle:$$

$$\dot{u}(x,t) = \frac{\omega H}{2}\frac{\cosh(ky)}{\sinh(kd)}\cos(kx - \omega t) \qquad (2.1.3)$$

$$Horizontal\ acceleration\ of\ wave\ particle:$$

$$\ddot{u}(x,t) = \frac{\omega^2 H}{2}\frac{\cosh(ky)}{\sinh(kd)}\sin(kx - \omega t) \qquad (2.1.4)$$

$$Vertical\ velocity\ of\ wave\ particle:$$

$$\dot{v}(x,t) = \frac{\omega H}{2}\frac{\sinh(ky)}{\sinh(kd)}\sin(kx - \omega t) \qquad (2.1.5)$$

$$Vertical\ acceleration\ of\ wave\ particle:$$

$$\ddot{v}(x,t) = -\frac{\omega^2 H}{2}\frac{\sinh(ky)}{\sinh(kd)}\cos(kx - \omega t) \qquad (2.1.6)$$

Full wave theories will require some modifications due to variable submergence at any given time (Chandrasekaran [5]). But basic form of the wave equation remains similar. The combined wave and current force for a shallow water wind turbine is about 3-6 MN according to Byrne and Houlsby (Figure 2.1.2).

## 2.2 Deep water foundation types

Using shallow water foundations such as jacket structure or monopoles in deep water will be very costly. Instead, floating structures are employed for deep water wind farms. There are primarily three types (Figure 2.2.1) of floating systems for offshore wind farms [7]:

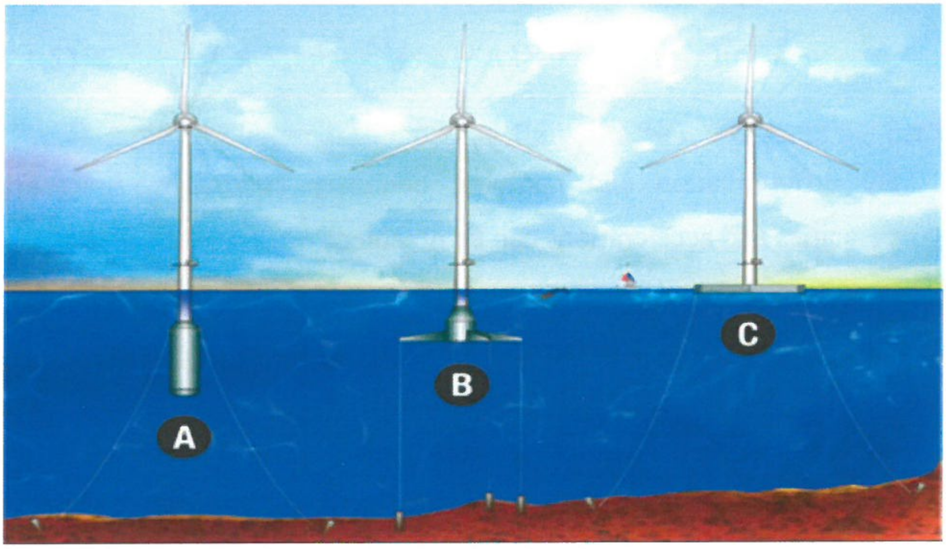


Figure 2.2.1 Types of floating systems: A. ballast stabilised "spar-buoy" with catenary mooring drag embedded anchors, B. Mooring line stabilised tension leg platform with suction pile anchors, C. Buoyancy stabilised "barge" with catenary mooring lines, [7]

A. Ballast stabilised (stabilisation by ballast) uses a heavy weight spar-buoy under water which provides counterbalance to the overturning moment from wind and wave loads. Mooring lines are loose and are simply used to keep the structure in place.
B. Tension leg platform (TLP, stabilisation by ties) uses highly tensioned mooring lines to keep the structure in place while ensuring stability at the same time.
C. Buoyancy stabilised (stabilisation by shape) uses a relatively large floating surface (a barge) to achieve stability. Mooring lines are loose and simply used to keep the structure in place.

The following sections will be used to discuss the merits and demerits of each types of floating substructure.

### 2.2.1 Ballast stabilised

Ballast stabilised foundations or spar buoys are currently being developed [7]. A good combination of a small water plane area and a large mass will ensure the stability of a wind turbine. Nevertheless, this is very hard technically. Wind turbines usually have a centre of mass high above the sea level. The spar buoy with a wind turbine on top need to have an overall centre of mass well below the sea level to achieve stability.

This then requires an extremely heavy buoy which makes transport and installation more difficult. A good balance between the dimensions of the spar buoy and the structural stability need to be achieved to be economic. Therefore, the major challenges are:

- Maximising pitch stiffness to minimise vessel heel
- Maximizing the natural heave period to reduce motion
- Minimising cost

### 2.2.2 Tension leg platform

Wind turbines with TLPs are lighter than ballast stabilised wind turbines and will allow more motion of the tower [7]. Heavy foundations and extremely high tensions in the mooring lines (each mooring line has $6.25\times10^6$ N in operation for MIT/NREL TLP [8]) are necessary in order to minimise the motion of the superstructure.

There are two major challenges for a TLP design. One challenge comes from the installation especially the tensioning of the platform. The other is on the design of anchoring- the anchors need to sustain large force so that they are stable in the soil.

### 2.2.3 Buoyancy stabilised

Buoyancy stabilised foundation uses a stabilised barge on the water surface to support superstructures. It is a lesser known foundation type for offshore wind turbine applications. It is highly susceptible to large waves [7]. Again, like any other floating structures, the challenges come from stability. Gyroscopic motion of the turbines makes it difficult to achieve stability.

### 2.2.4 Choice of foundation type

TLPs are considered to have the most potential for success over the other types of floating structures in terms of both technology and economical potentials. The TLP concept has less tilting motions compared to the other two concepts. According to

Casale, Lembo, et al., the construction and installation process of TLP structures have proven to be the most effective and economically viable technique [9].

Figure 2.2.2 includes some sketches illustrating the typical movements that these three floating systems will have under wind [9]. Ballast stabilised and buoyancy stabilised floating wind turbines have primarily translational and tilting motions while TLPWTs are restrained by tensioned mooring lines and make horizontal shifts only. Too much tilting motions will lead to reduction in power output and may limit the operation of power generation [10].

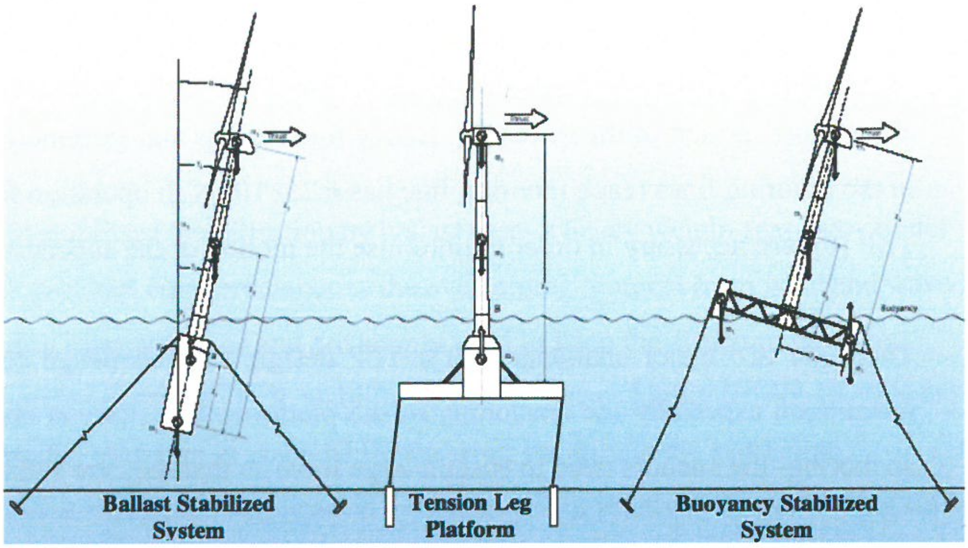


Figure 2.2.2 Typical movements of different floating wind turbines, [9]

Therefore, due to its ease of construction and higher stability with lower economic cost, the TLP floating system is the most viable design for a floating offshore wind turbine. TLP has thus been chosen as the floating system in this project.

## 2.3 Analysis method

In the analysis conducted by Matha [11], the computational analysis of a 5-MW TLP wind turbine was conducted using design code FAST (Fatigue, Aerodynamics, Structures, and Turbulence or FAST is the design code of National Renewable Energy Lab). A right-handed Cartesian coordinate system (X, Y, Z) was defined. The rotational motions (roll, pitch, yaw) and translational motions (surge, sway, heave) have also been defined. This definition is shown as Figure 2.3.2. It was found that the TLP system oscillates in surge from -1 m to 8 m. This oscillation occurred at the natural surge frequency of the structure and was caused by the rotor thrust which, in turn, was caused by the varying blade pitch. The time series of motions showed that the surge oscillation also excited the other 5 degrees of freedom by couplings with the mooring lines (Figure 2.3.2).

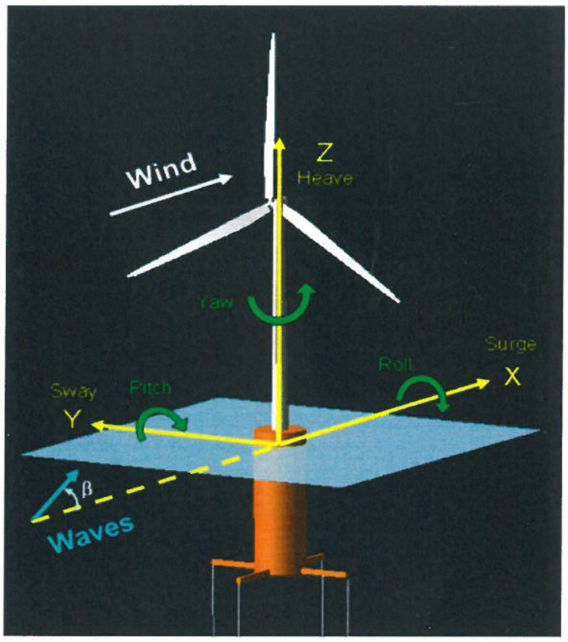


Figure 2.3.1 Definition of the coordinate system and motions, [11]

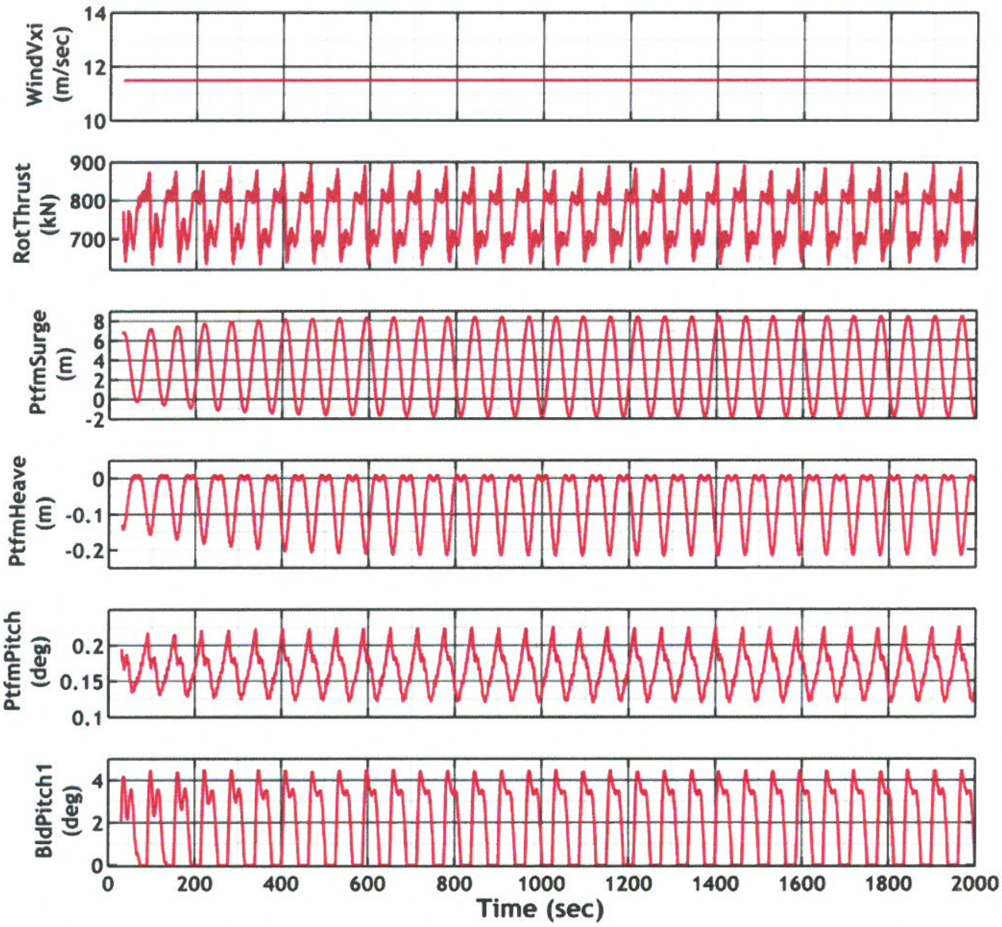


Figure 2.3.2 Time response of rotor, platform and blade of a 5-MW TLP wind turbine due to a constant speed wind, [11]

A software simulation is a good starting point for a design with minimum cost, but lacks the validity of physical proof. The method used in this analysis enabled the thoughts on using micro sensors on a physical model to analyse the motions of a TLP system. The analysis that Matha [11] conducted was based on a full scale TLP supporting a wind turbine and should yield good results. In contrast, a rudimentary physical model may not be as accurate as a computational model initially, but improvements can be made step by step to achieve the ultimate scaled-down version of a TLPWT.

## 2.4 Past experiments

Daniel [12] has pioneered the TLP floating system model with a floating box made out of steel. The setup is shown as Figure 2.4.1. The floating box is 175 mm wide, 175 mm long and 225 mm in height. With a self-weight of 1.593 kg, it can stay afloat with 53 mm depth of water displaced. There are four accelerometers (MEMS) attached on the surface of the floating box, and one load cell measuring the tension within one of the four mooring lines. The floating system is moored using fixed connections with the water tank as shown in Figure 2.4.2. The whole water tank sits on a shaking table which can be controlled to shake at certain frequencies.

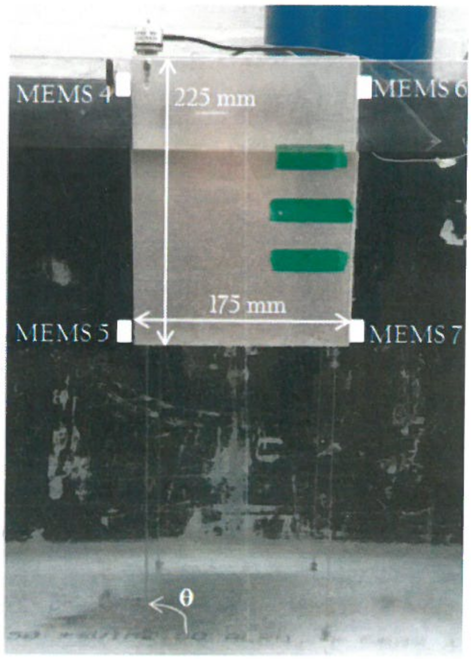


Figure 2.4.1 Initial TLP floating system model, [12]

The full details of the setup are explained in Section 3.1 of this report. The setup shown in Figure 2.4.2 is the same as the preliminary experiment of this project.

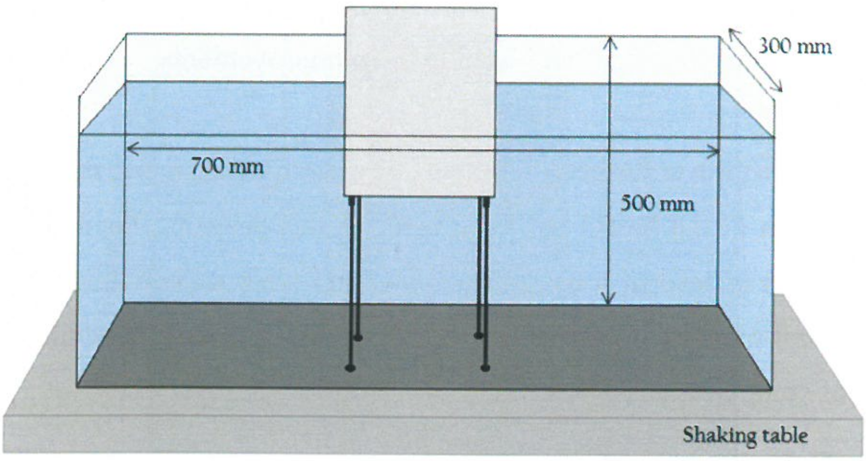


Figure 2.4.2 Overview of the experimental setup, [12]

Daniel [12] has used a method of obtaining the natural frequency of the system by incrementally raise the applied frequency of the shaking table. By applying frequencies with increments of 0.01 Hz, she was able to get Figure 2.4.3 in which maximum acceleration is plotted against the applied frequency. It is clear that around 1.14 Hz the accelerations are the largest. Therefore, the natural frequency (or more precisely, the first mode of resonance) was concluded to be around 1.14 Hz.

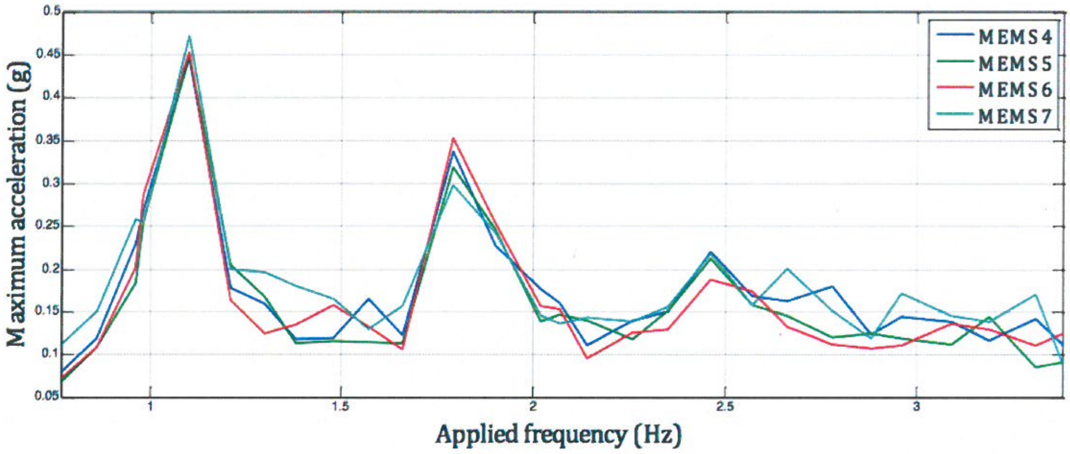


Figure 2.4.3 Maximum acceleration at different applied frequencies, [12]

Her experiments also included some other frequency analysis, and some comparisons between different mooring setups to evaluate stability of the system. Overall, she has given a very successful starting point which allows future researchers to look into the TLP modelling techniques with step-by-step improvements.

With the intention to further investigate the system performance metrics of a TLP model, modification of the model has been made in this project. This includes a light-weight Perspex box instead of a heavy steel one, and plate anchor foundation instead of fix-ended mooring. By employing similar acceleration and tension monitoring scheme, other types of comparisons are possible.

# 3. Experimental setup, techniques used and theory

## 3.1 Overview of the experiment

Figure 3.1.1 Photo taken for the Perspex box TLP model

Figure 3.1.1 is a photo taken as one of the experiments was in progress. This setup used a Perspex box instead of the steel box used previously in Daniel's experiment (Figure 2.4.1) [12].

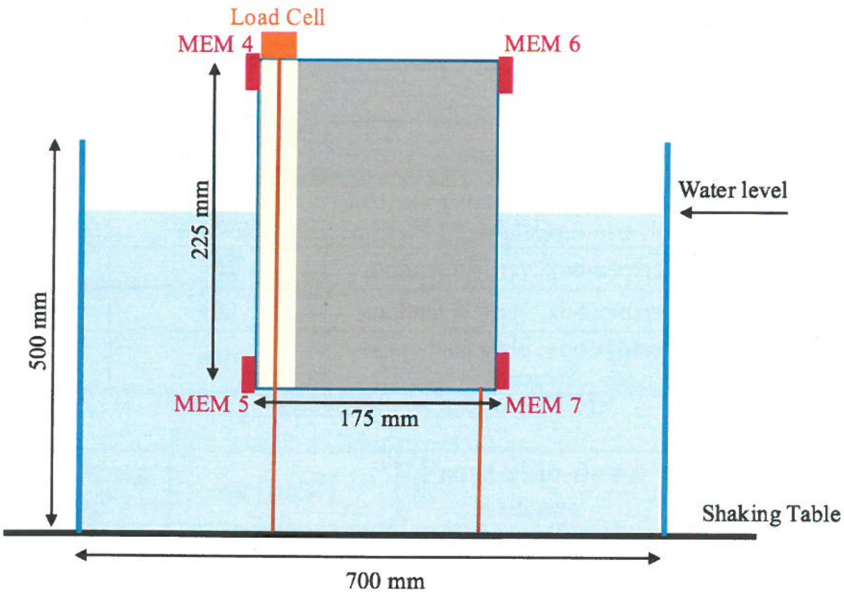


Figure 3.1.2 Experimental setup overview (experiment 1, 2 and 3)

Figure 3.1.2 is an overview of the experimental setup. Overall, it consists of a floating box with four tendons acting as mooring cables, and a large water tank sitting on a shaking table which generates simulated ocean waves. A plastic tube is installed to allow the load cell to be attached to the tendon. The setup in Figure 3.1.2 are for the first stage (experiment 1, 2 and 3 as described in Table 3.1.1) where the mooring lines are directly fixed onto the bottom of the water tank. There are several sensors attached to the setup:

1. Accelerometers (or MEMS, micro-electrical-mechanical system) are attached to the outer surface of the box. These MEMS only measures 1D horizontal accelerations.
2. A load cell is installed at the end of one of the tendons. It is able to monitor the tensions continuously.

The motion of the shaking table will be horizontal. Generated acceleration of the water tank will be transferred to the water inside, and hence the floating system will be impacted by waves. The frequency of shaking can be controlled via a control panel and can be set between 0 to 5 Hz with a minimum increment of 0.01 Hz.

There are several experiments performed and will be described in details in the following sections. The key parameters are summarised in Table 3.1.1. Experiment numbers will be used when necessary in this report.

Table 3.1.1 Summary of key parameters of experiments

| Experiment number | Setup type | Tendon length (mm) | Depth of water displaced (mm) |
|---|---|---|---|
| 1 | Steel box (preliminary), vertical tendons | 205 | 151 |
| 2 | Perspex box, vertical tendons | 205 | 151 |
| 3 | Perspex box, vertical tendons | 205 | 120 |
| 4 | Perspex box, plate anchors in sand | 310 | 90 |

## 3.2 Preliminary experiment (experiment 1) setup

### 3.2.1 Overview of the preliminary experiment

The preliminary experiment (experiment 1) has been done with a steel floating box weighing 1.593 kg. The setup has been shown in Figure 3.1.2. The sensors have been used to successfully record the accelerations and tensions over time. This experiment has demonstrated the validity of extraction of useful system metrics from a box TLP model.

### 3.2.2 Calibration of apparatus

Before each set of experiments is conducted, all the sensors need to be calibrated so that voltage outputs can be converted into physical values. In this setup, the voltage readings of MEMS need to be converted into accelerations ($m/s^2$) while readings of the load cell need to be converted into tension (N).

Since the near-linearity of the MEMS, the calibration of MEMS can be simply done by flipping the orientation of the MEMS by 180°. This will give one voltage reading at 'positive' gravitational acceleration and one voltage reading at 'negative' gravitational acceleration. Table 3.2.1 is the calibration table of four MEMS for the preliminary experiment (experiment 1). The two orientations of the floating box are called 'front side up' and 'front side down'- this simply means the floating box is flipped by 180°. It can be seen that there is very small inconsistency of the voltage readings between a pair of MEMS (e.g. MEM4 and MEM5 are both on the same side). So the calibration results should be valid.

Table 3.2.1 Calibration table of the MEMS

| Transducer | Front-side-up voltage | g ($m/s^2$) | Front-side-down voltage | g ($m/s^2$) |
|---|---|---|---|---|
| MEM4 | 1.4948 | 9.81 | 3.4506 | -9.81 |
| MEM5 | 1.4941 | 9.81 | 3.4402 | -9.81 |
| MEM6 | 3.4062 | -9.81 | 1.4779 | 9.81 |
| MEM7 | 3.3831 | -9.81 | 1.4397 | 9.81 |

As a result, the calibration equation can be concluded from the calibration chart of each MEMS. An example of the MEM4 calibration chart is given as Figure 3.2.1. The calibration equation can then be used in the data analysis.

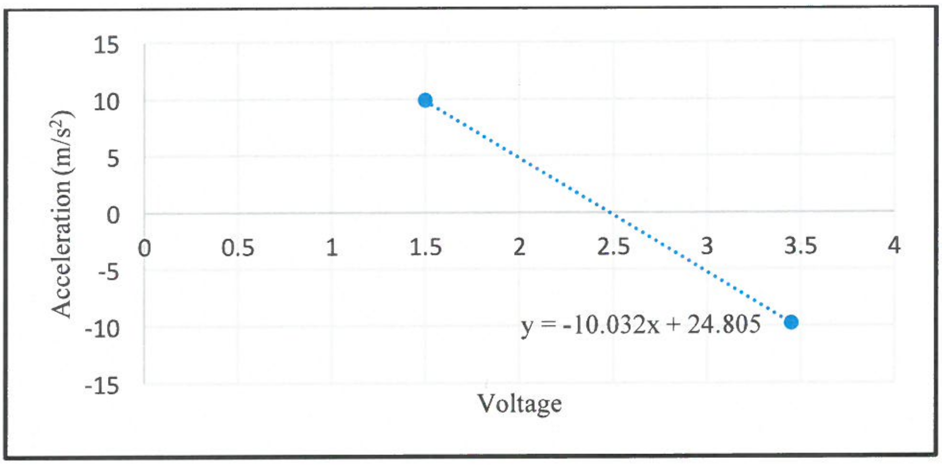


Figure 3.2.1 MEM4 calibration chart (voltage-acceleration conversion)

The calibration of the load cell can be done with gradual increase of depth of water displaced (h) by the floating box. By knowing the h (hence the buoyancy) and the weight of the box, the tension of each mooring line can be calculated (Figure 3.3.2). A series of tension values and respective voltages can be used to plot a calibration chart. Figure 3.2.2 is the calibration chart of the load cell for the preliminary experiment.

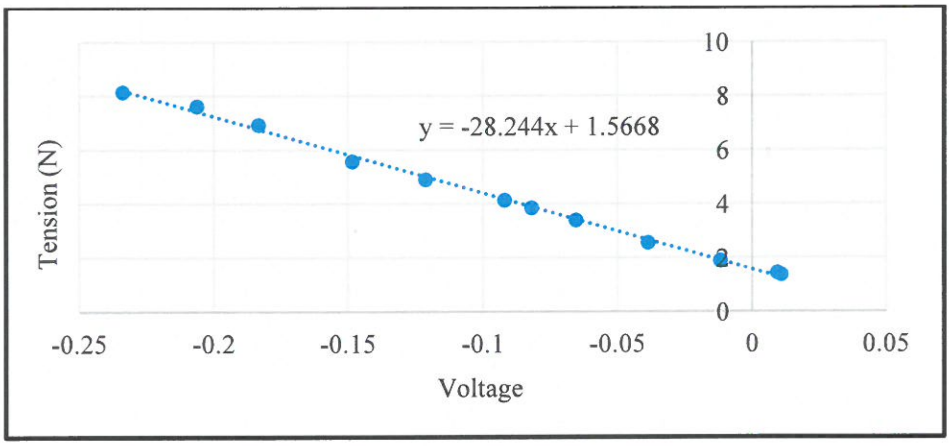


Figure 3.2.2 Calibration chart for the load cell (voltage-tension conversion)

The calibration methods are similar for the improved experiment setups in experiment 2, 3 and 4.

### 3.2.3 Data acquisition and signal processing

Figure 3.2.3 illustrates the data acquisition process for the equipment. All the signals from MEMS and load cell were input into a junction box which acts as an amplifier, an analogue filter and a power supply. Then the treated signals were sent into a data logger (a desktop PC with specialised connectors). The software on the desktop PC would record all the electrical signals in voltages over time into a text file. The recording used a sampling rate of 2000 Hz to eliminate aliasing. The text files will eventually be processed by using MATLAB.

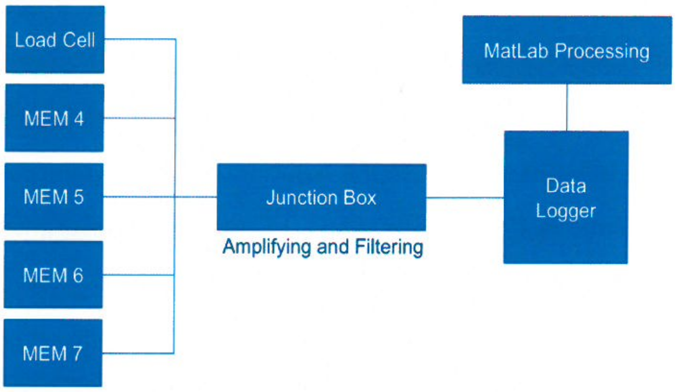


Figure 3.2.3 Data acquisition system

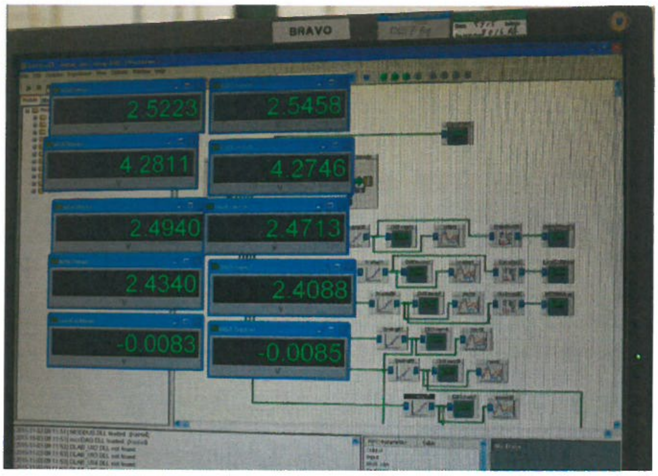


Figure 3.2.4 Data logging software

On MATLAB, the signals recorded will be treated with a Butterworth filter which is basically a low pass filter. This digital filter will eliminate the frequency contents higher than 30 Hz (cut-off frequency) so that the resulted signals will be useful for the purpose of this project. A 'filtfilt' function was also used to 'zero' the phase difference by passing signals in forward and reverse directions into the same filter. The filtered voltage signals would then be calibrated to physical quantities (acceleration and tension) to plot figures.

## 3.3 Improved experiment setups

### 3.3.1 Overview of the improved experiment setups

There are two stages of the improved experiments. In the first stage (experiment 2 and 3), a Perspex box weighing 1.212 kg has been made to match the dimensions of the steel box (more details in Section 3.3.2). A lighter floating box will result in a higher tension within the tendons at the same volume of water displaced (Figure 3.3.2). This increase in tension will affect the behaviour of the system. A light-weight floating box will also enable the investigation of the box weight contribution to the overall performance metrics.

In the second stage (experiment 4), major changes have been made to the foundation of the TLP model. Instead of using unrealistic fix-ended tendons, plate anchors have been developed (Figure 3.3.1). These plate anchors are essentially copper plates with radius of 5 cm and thickness of 1 cm. The tendons are installed onto the centres of the plate anchors, and the anchors are embedded in Hostun sand to provide strength. The superstructure of the setup will remain the same configuration as shown in Figure 3.1.2. In terms of design, the embedment calculation has been made and will be demonstrated in Section 3.3.3.

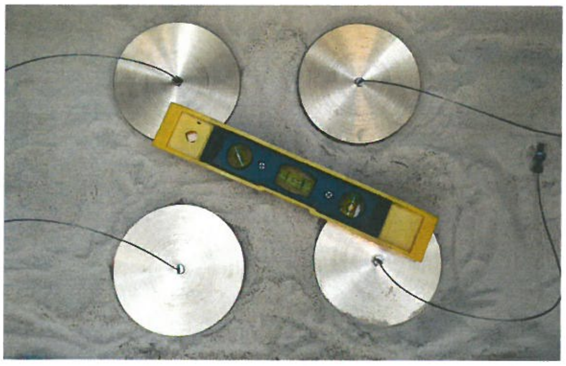

Figure 3.3.1 Copper plate placed over a thin layer of sand, to be used for anchoring in experiment 4

### 3.3.2 Perspex box design and controlled variables

The new Perspex box has been designed to fit the purpose of the experiment 2, 3 and 4. For experiment 2, several variables need to be controlled to conclude the performance differences with different box weights: tendon length, dimensions of the box and cable connection method. Therefore, the Perspex box has been designed to have the same dimensions as the steel box (175 mm × 175 mm × 225 mm). Tendons with the same lengths (205 mm) have been used, and all the sensors have been transplanted onto the Perspex box with locations being the same.

The volume of water displaced or the depth of water displaced by the box also need to be controlled. There are two reasoning towards this argument:

1. Several forces including a buoyancy, a weight and four tensions in the tendons are in balance when the box is static. This can be illustrated by the static force balance diagram in Figure 3.3.2. The buoyancy needs to be kept the same as before. With the same buoyancy, a lighter weight Perspex box means higher tensions in the tendons. This is allowable as the weight differences are physically compensated by the variations in tensions.

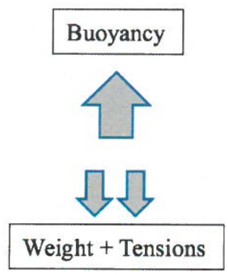

Figure 3.3.2 Static force balance diagram of floating box

2. Fluid damping effect when the box is in motion. Although this project does not involve much insight into the fluid dynamics, it is obvious that with the floating box in motion, water in the proximity of the box will provide a large damping effect. A dramatic slow-down of motion of the box was also observed when the shaking table is switched off after shaking. This damping effect will correlate strongly with the depth of water displaced, therefore the depth need to be controlled.

The depth of water displaced is thus set to 151 mm for both the preliminary experiment with steel box (experiment 1) and the improved experiment with Perspex box (experiment 2 and 3).

### 3.3.3 Embedment calculation

Figure 3.3.3 illustrates the layout of experiment 4 with embedment depth D and depth of water displaced h. The depth of embedment needs to be considered according to the following factors:

1. The weight of sand above the plate anchor and the weight of the anchor itself.
2. Factor of safety. To ensure the safety of the system, a factor of safety need to be set to 1.5. According to the force balance of a single anchor (Figure 3.3.2), the factor of safety is defined as Eq. 3.1.1.

$$\text{FoS} = \frac{Tension\ T}{Weight\ of\ anchor\ W_A + weight\ of\ sand\ W_S} \qquad (3.3.1)$$

3. The relative density of the sand $I_D$. $I_D$ varies a lot for Hostun sand and need to be controlled carefully.

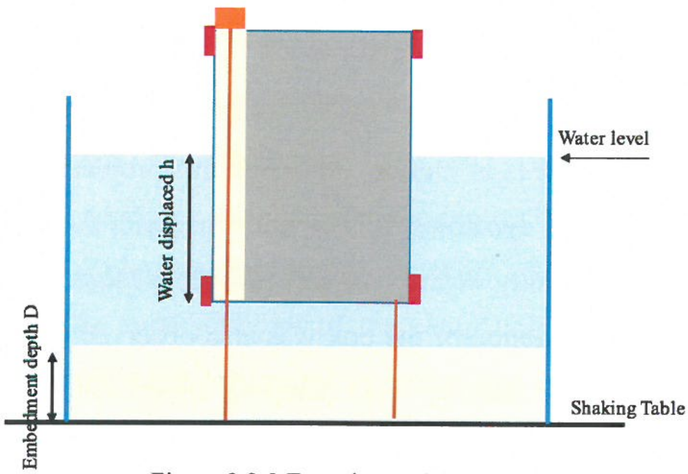

Figure 3.3.3 Experiment 4 setup

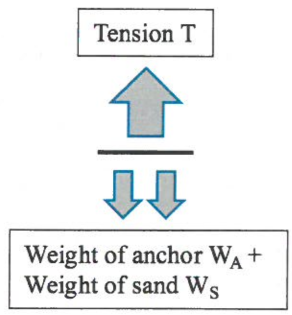

Figure 3.3.4 Force balance of an anchor

To get the weight of sand $W_S$ above the anchors, it is necessary to get the dry unit weight of the sand $\gamma'_s$. It can be obtained using Eq. 3.3.2 where $G_S$ is the specific gravity, e is the void ratio of sand and $\gamma_w$ is the unit weight of water.

$$\gamma'_s = \frac{G_S - 1}{1 + e} \times \gamma_W \qquad (3.3.2)$$

It has been determined that the void ratio of the sand was 0.603 by using a test pouring (more details in Section 3.3.4). Sand usually has a specific gravity $G_S$ of 2.65. The dry unit weight $\gamma'_s$ is then calculated to be 10.10 kN/m$^3$.

By expanding Eq. 3.3.1, a better insight of the relationships can be obtained as Eq. 3.3.3. 8500 kg/m$^3$ is the density of copper used, t and r are the thickness and radius of the plate anchors. Therefore, the key parameters are embedment depth D, geometry of anchor plate and tension T.

$$FoS = \frac{\pi r^2 D\gamma'_s + \pi r^2 t \times 8500g}{T} \qquad (3.3.3)$$

Although the static tension of each tendon is relatively low, there is an increase in the tension when the TLP is in motion. It was observed that the tension can get up to twice as large as the static value in the preliminary experiment (Table 3.3.1). Dynamic amplification factor is defined in Eq. 3.3.4. A DAF of 2 can be concluded.

$$\text{DAF} = \frac{Static\ load}{Dynamic\ peak\ load} \qquad (3.3.4)$$

Table 3.3.1 Dynamic amplification factor calculation

| Static load at 151 mm | Dynamic peak load at 151 mm | DAF |
|---|---|---|
| 7.58 N | 15.21 N | 2 |

With some safety consideration, it is necessary for tensions to be multiplied by 3 to compensate for the changes in DAF values.

After some calculations, it has been determined that a combination of D, h (which will affect T), r and t will yield a good solution to the problem. This combination of parameters has been summarised in Table 3.3.2.

Table 3.3.2 Summary of key parameters of embedment design

| D (mm) | r (mm) | t (mm) | h (mm) | $T_{static}$ (N) | $T_{peak}$ (N) |
|---|---|---|---|---|---|
| 180 | 50 | 10 | 90 | 4.5 | 13.5 |

**N.B.** *D: depth of embedment, r: radius of the plate anchors, t: thickness of the plate anchors, h: depth of water displaced,* $T_{static}$*: static load at h=90 mm,* $T_{peak}$*: dynamic peak load at h=90 mm*

For a single plate anchor, the weight of the anchor is 6.47 N and the weight of 18 cm embedment is 14.28 N. With a peak tension set to be 13.5 N (dynamically amplified load), and by using Eq. 3.3.1, a reasonably high safety factor of 1.54 can be concluded.

### 3.3.4 Sand (Hostun) preparation

The sand which will be used to bury the plate anchors will need to be poured according to certain criteria such that dry unit weight $\gamma'_s$ can be controlled to be 10.10 kN/m$^3$. Figure 3.3.5 shows the sand pouring equipment. It consists of a large funnel containing sand and a guide tube which allows sand to be poured onto the required surface within the tank beneath.

Figure 3.3.5 Sand pouring equipment

Figure 3.3.6 The aperture at the bottom of the funnel

There are two parameters of the equipment that need to be set to achieve the target 10.10 kN/m$^3$ unit weight. One is the aperture size at the bottom of the funnel (Figure 3.3.6 shows the aperture). It controls the rate of the sand flow (mass/time). The other is the height of pouring. The rate of the sand flow and the height of pouring will both impact the compaction of sand hence influence the resulted unit weight of sand.

By Eq. 3.3.2, with the knowledge of the void ratio, the unit weight of sand can be determined. The void ratio is controlled by the compaction of the sand, and can be determined by a calibration pouring. A series of calibration pouring was conducted so that a good combination of aperture size and pouring height can be determined. It was found out that when the bottom of the funnel is positioned at a height of 135 cm above the sand surface, and when the aperture size is set to 11 mm, the dry unit weight of sand will be around 10.10 kN/m$^3$. Table 3.3.3 shows the parameters for the adopted calibration pouring and the resulted void ratio.

Table 3.3.3 Parameters for the adopted calibration pouring and yielded void ratio

| **Aperture size** | **Pouring height** | **Volume of sand for calibration $V_T$** | **Mass of sand for calibration $M_S$** | **Yielded void ratio e** |
|---|---|---|---|---|
| 11 mm | 135 cm | 200 ml | 0.33 kg | 0.603 |

Eq. 3.3.5 is used to conclude the void ratio (e) from the volume and mass of sand. The sand pouring can then be conducted with this guidance. By plugging the void ratio 0.603 into Eq. 3.3.2, the dry unit weight of sand is 10.10 kN/m$^3$.

$$e = \frac{V_T}{V_S} - 1 = \frac{V_T}{M_S \div (G_S \rho_W)} - 1 = 0.603 \qquad (3.3.5)$$

# 4. Results and discussions

## 4.1 Preliminary experiment (experiment 1)

In the preliminary experiment (experiment 1), the original steel box was used. Key parameters of experiment 1 are summarised again in Table 4.1.1. The purpose of this experiment is to validate the sensor application and to conclude an acceptable experimental method. To achieve that, the aim of experiment 1 is set to finding the natural frequency (or more precisely, the first mode of resonance) of the system with the key parameters set to those in Table 4.1.1.

Table 4.1.1 Summary of key parameters of experiment 1

| Experiment number | Setup type | Tendon length (mm) | Depth of water displaced (mm) |
|---|---|---|---|
| 1 | Steel box (preliminary), vertical tendons | 205 | 151 |

To find the natural frequency of the system, incremental frequencies need to be applied. It was decided that the range was set within 0 to 2 Hz since in Daniel's [12] experiment, the natural frequency was determined to be 1.14 Hz at 80 mm of depth of water displaced. Since experiment 1 is only a validation of the experimental method, the accuracy of the result is trivial- the natural frequency has already been determined by Daniel. Therefore, a relatively large frequency increment of 0.25 Hz was used.

After recording all the acceleration and tension readings at all the frequency steps from 0 to 2 Hz, data were processed and graphs were plotted. It is important to extract the steady state data where the TLP model is physically shaken at the applied frequency. In this steady state, the amplitude should also be constant.

### 4.1.1 Acceleration of the TLP system

Figure 4.1.1 is a typical time domain plot of the acceleration. It includes the accelerations measured by MEM4 between 40 s and 55 s after shaking started. Although the peaks are noisy it is still very clear that the periodical motion has been recorded successfully. The peak acceleration is around ±2.58 $m/s^2$.

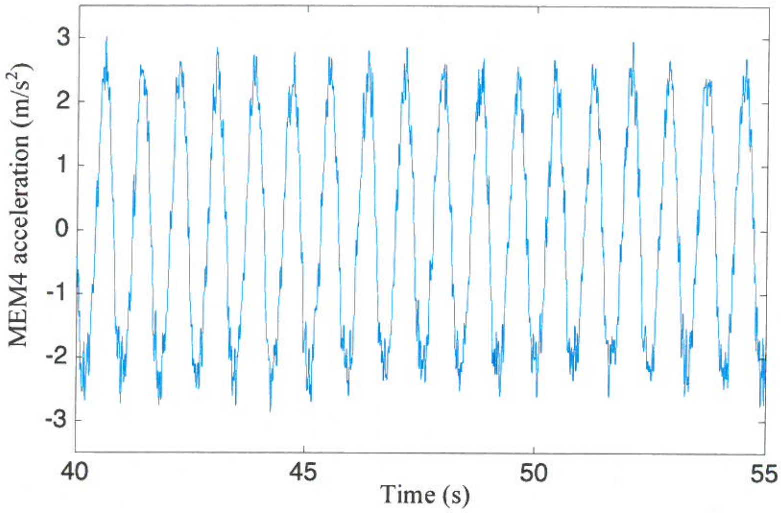


Figure 4.1.1 Time domain plot of MEM4 between 40 s and 55 s at 1.25 Hz applied frequency (experiment 1)

By applying Fourier transform to Figure 4.1.1, a frequency domain plot can be obtained as Figure 4.1.2. The vertical axis of the frequency domain has been adjusted such that the magnitude represents the exact acceleration amplitude in the units of m/s$^2$. From Figure 4.1.2, it is clear that the peak occurred at the frequency of 1.233 Hz instead of 1.25 Hz. This is due to the system error of the shaking table- the control panel value (set to 1.25 Hz) for the shaking table always has some deviation from the values read from frequency domain plots by MATLAB.

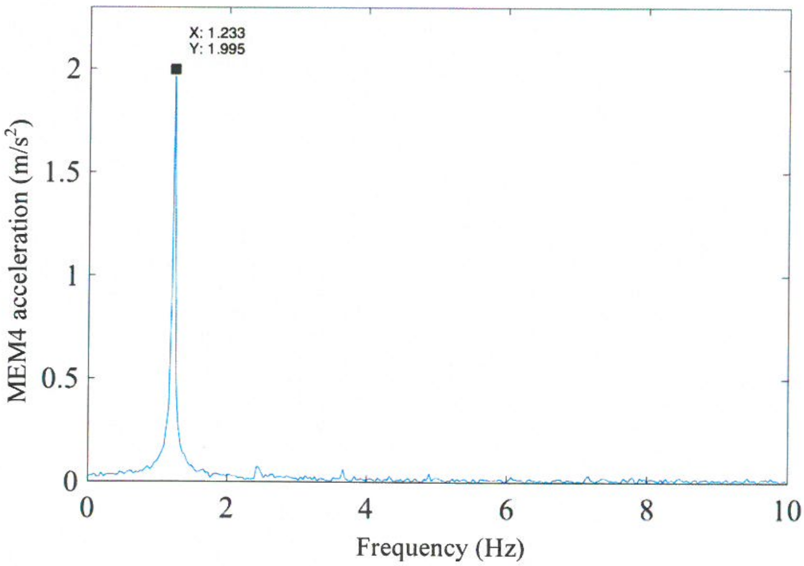


Figure 4.1.2 Frequency domain plot of MEM4 at 1.25 Hz applied frequency (experiment 1)

To conclude a natural frequency of the system, it is necessary to look at the peak accelerations at all frequency steps. By using the same method as above (Figure 4.1.1 and Figure 4.1.2), both the time domain and frequency domain at all frequencies were plotted. For MEM4, the summary plot of peak accelerations at all frequencies is given as Figure 4.1.3.

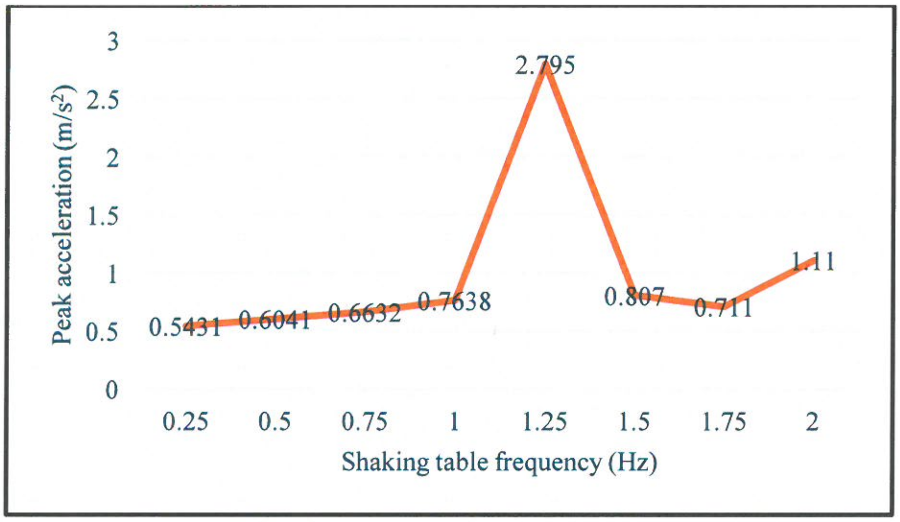


Figure 4.1.3 MEM4 peak acceleration at different frequencies (experiment 1, depth of water displaced=151 mm, static tension in tendon=7.58 N)

It can be seen that when the shaking table was set to 1.25 Hz, the peak acceleration reached 2.795 $m/s^2$. This is the natural frequency (or first mode of resonance). But since the frequency steps are 0.25 Hz, it can only be said conservatively that the natural frequency should occur at a frequency between 1 Hz and 1.5 Hz. The second peak seems to occur at around 2 Hz as there is a tendency of increase.

Figure 4.1.4 includes the peak amplitudes ($m/s^2$) in frequency domain plots for MEM4. The frequency content of 0.25 Hz and 0.5 Hz were too low to be read hence neglected. The maximum amplitude occurred at 1.25 Hz again. This can verify the result obtained from Figure 4.1.3.

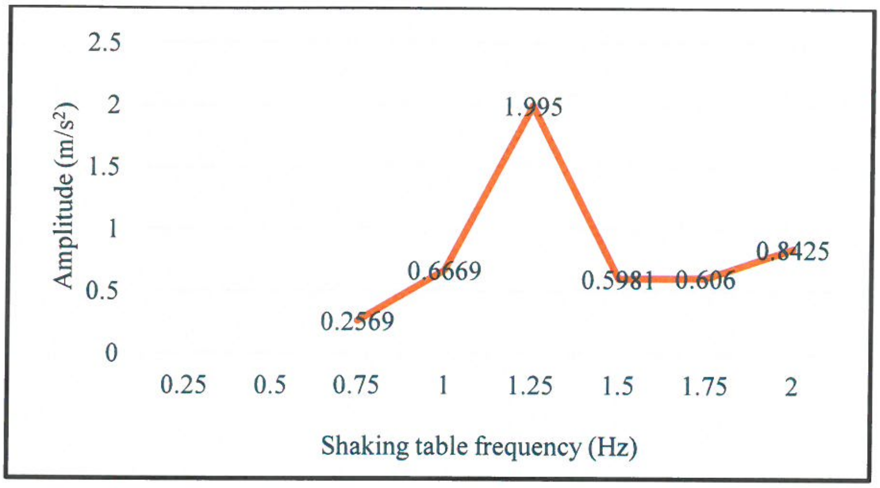


Figure 4.1.4 Peak amplitude in frequency domain for MEM4 (experiment 1, depth of water displaced=151 mm, static tension in tendon=7.58 N)

Nevertheless, there is some deviation of the magnitude- 2.795 $m/s^2$ in Figure 4.1.3 while 1.995 $m/s^2$ in Figure 4.1.4. This is due to the inaccuracy of directly reading the peak accelerations from time domain plots (e.g. the one in Figure 4.1.1). There are always some variations in peak accelerations in time domain as the plots are not smooth. The frequency domain magnitude is not purely concluded from the applied frequency 1.25 Hz but with other noise as well- this may affect the magnitude of the peak.

Similar techniques were also applied to MEM5, MEM6 and MEM7. All the results lead to the conclusion that natural frequency is between 1 Hz and 1.5 Hz.

### 4.1.2 Tension of the mooring line

Similarly, tension of the tendons can also be plotted in time domain. This is shown as Figure 4.1.5. It can be seen that the tension is roughly between 2 N and 15 N. The value 7.58 N (red line) is the static tension when the TLP system is balanced under tension, buoyancy and self-weight.

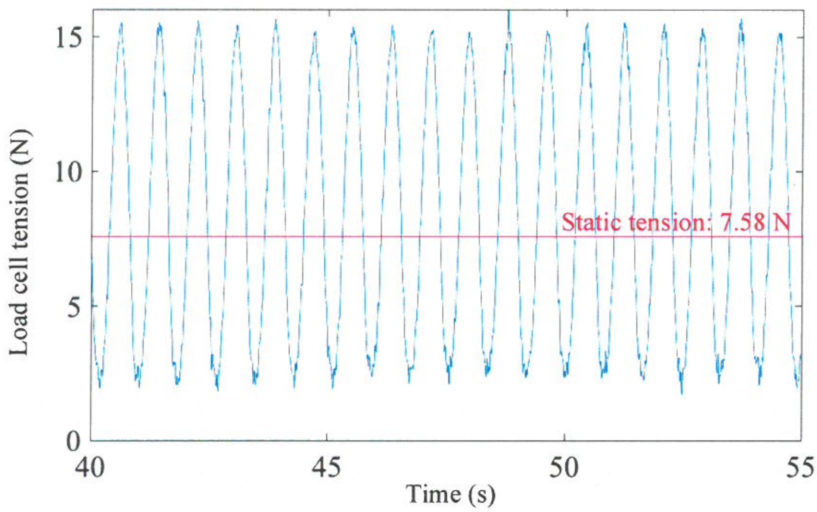


Figure 4.1.5 Time domain plot of load cell between 40 s and 55 s at 1.25 Hz applied frequency (experiment 1)

There is some deviation from symmetry when looking at the lower part of the plot in Figure 4.1.5- the 'lower half' of the plot is smaller than the 'upper half'. This may be explained by the compression of the load cell attachment when the force within the load cell is changing dramatically. Later in experiment 2, more dramatic change (Figure 4.2.3) will be observed.

The Fourier transform can also be applied to the time domain of tension plot to get the frequency domain, and this is given as Figure 4.1.6.

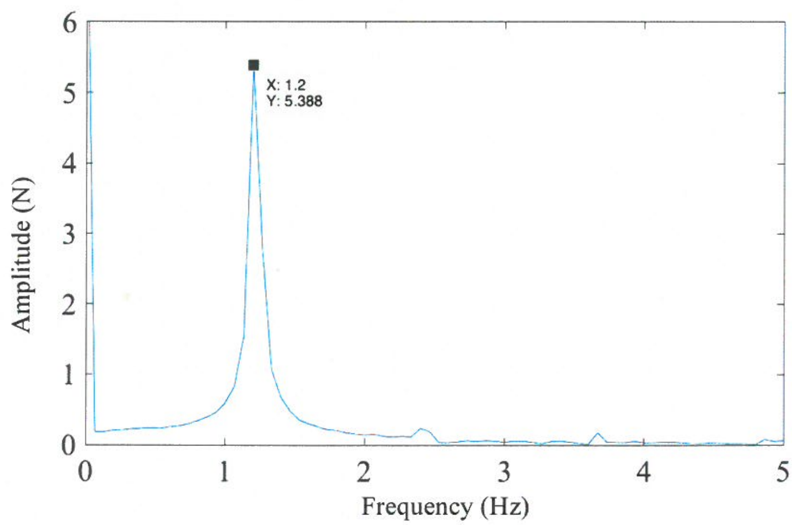


Figure 4.1.6 Frequency domain plot of load cell at 1.25 Hz applied frequency (experiment 1)

The Fourier amplitude at 1.25 Hz applied frequency (or 1.20 Hz as read from Figure 4.1.6) is 5.388 N. Similar to the frequency domain for MEM4 acceleration (Figure 4.1.2), this peak describes the amplitude of the time domain plot. From the time domain plot for tension (Figure 4.1.5), the amplitude is (15-2)/2=6.5 N. This is close to the peak value of 5.388 N read from Figure 4.1.6. Again, the difference is due to the variable peak accelerations in Figure 4.1.5 and random noise.

Similar conclusion of the natural frequency can also be drawn from the plots of peak tensions against all frequency steps (Figure 4.1.7), and Fourier amplitudes against all frequency steps (Figure 4.1.8).

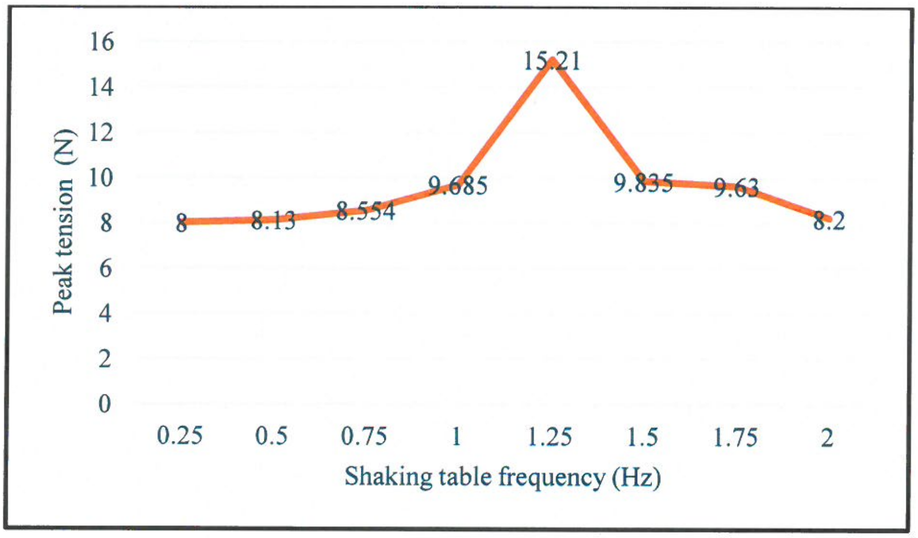


Figure 4.1.7 Load cell peak tension at different frequencies (experiment 1, depth of water displaced=151 mm, static tension in tendon=7.58 N)

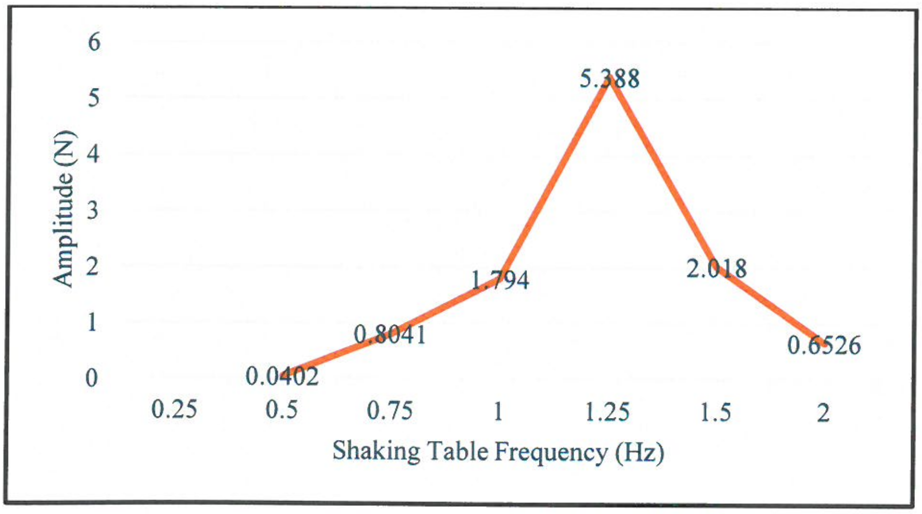


Figure 4.1.8 Peak amplitude in frequency domain for MEM4 (experiment 1, depth of water displaced=151 mm, static tension in tendon=7.58 N)

From Figure 4.1.7 and Figure 4.1.8, it can be concluded again that the largest tension occurred at 1.25 Hz. This consolidated the conclusion that the natural frequency (first mode of resonance) is between 1 Hz and 1.5 Hz.

### 4.1.3 Conclusions from the preliminary experiment (experiment 1)

The preliminary experiment has determined an effective method to record, analyse and present acceleration and tension. Similar method will be adopted for the other experiments.

The method of finding the natural frequency of the TLP system is valid. This experiment was carried out at 151 mm of depth of water displaced, so it may not be scientific to directly compare the result with Daniel's. But the result obtained by Daniel (natural frequency=1.14 Hz at 80 mm water depth, [12]) is within the range of 1 and 1.5 Hz.

It is necessary to increase the accuracy of the result. As it was possible to set the shaking table frequency to an accuracy of 0.01 Hz, it was decided that in experiment 2 (reference to Table 3.1.1) where the new Perspex box will be used, a frequency increment of 0.1 Hz would be used.

## 4.2 Perspex floating system with vertical fix-ended mooring cables (experiment 2 and 3)

In experiment 2 and 3, the setup is exactly the same as experiment 1 (Figure 3.1.2). Table 4.2.1 summarises the key parameters of experiment 1, 2 and 3. The only difference between experiment 1 and 2 is that the new Perspex box has been used instead of the steel box. For experiment 3, the depth of water displaced is changed from 151 mm to 120 mm to investigate the effect of water depth.

Table 4.2.1 Summary of key parameters of experiment 1, 2 and 3

| Experiment number | Setup type | Tendon length (mm) | Depth of water displaced (mm) |
|---|---|---|---|
| 1 | Steel box (preliminary), vertical tendons | 205 | 151 |
| 2 | Perspex box, vertical tendons | 205 | 151 |
| 3 | Perspex box, vertical tendons | 205 | 120 |

### 4.2.1 Comparison of experiment 1 and experiment 2

For experiment 2, the time domain and frequency domain plots for the MEM4 acceleration measured at 1.25 Hz Perspex box setup are given as Figure 4.2.1 and Figure 4.2.2. By reading from Figure 4.2.2, the actual frequency applied is 1.267 Hz. This is close enough to the 1.233 Hz observed in Figure 4.1.2 (experiment 1) to enable the comparison. However, note that the 1.25 Hz here may not be the natural frequency of the Perspex system. With the same applied frequency and different mass of the floating box, a comparison of the system response to different mass can be made.

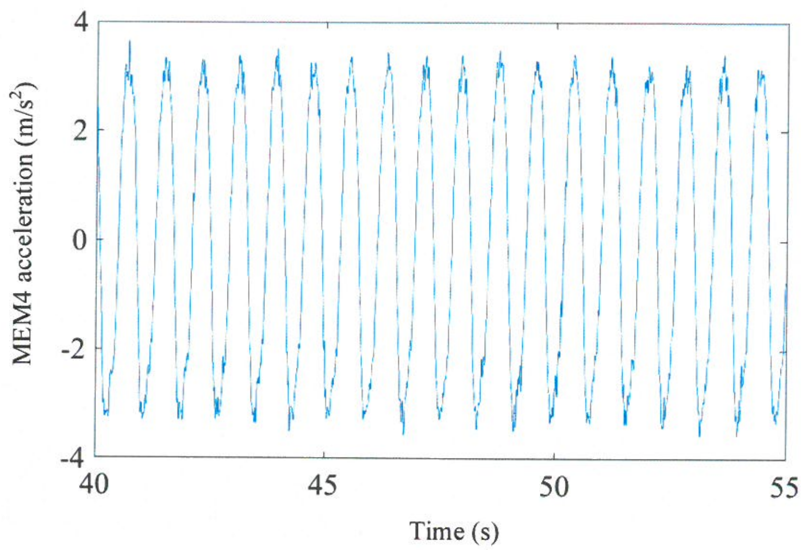


Figure 4.2.1 Time domain plot of MEM4 between 40 s and 55 s at 1.25 Hz applied frequency (experiment 2)

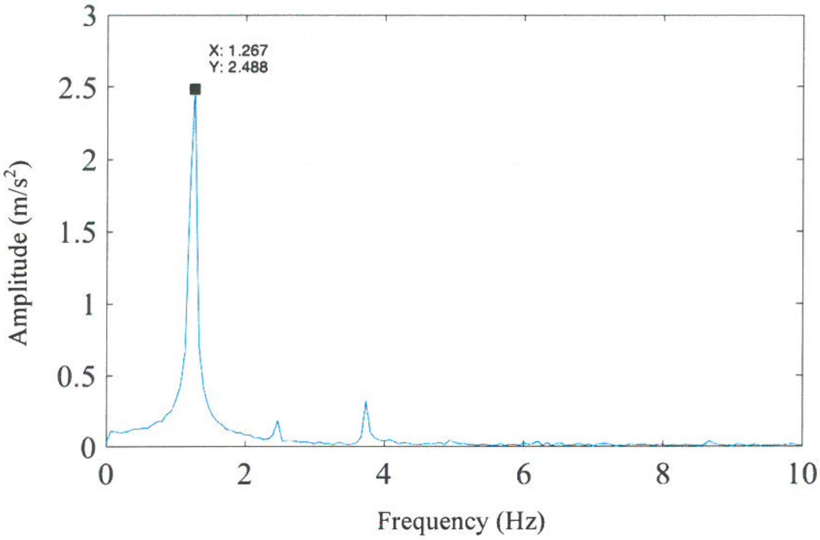


Figure 4.2.2 Frequency domain plot of MEM4 at 1.25 Hz applied frequency (experiment 2)

From Figure 4.2.1, the maximum acceleration is around ±3.25 m/s$^2$. Therefore, it is about 16% larger than the same setup with the original steel box (From Figure 4.1.1, the maximum acceleration is around ±2.58 m/s$^2$).

This maximum acceleration difference can be interpreted as 'a lighter weight floating system will have a higher acceleration response in the same ocean wave'. From the energy point of view, this can be thought of as an energy conservation problem: when a system is oscillated by the same external force (wave force), a light weight object must have a higher kinetic energy so that the total mechanical energy will be the same as a heavy weight object.

Figure 4.2.3 shows the tension recorded between 40 s and 55 s. As mentioned earlier in Section 4.1.2, asymmetry of the tension plot is due to the compression of the load cell connection. Due to a more flexible connection made from Perspex, this effect is enlarged. The plot in Figure 4.2.3 looks not symmetrical at all- the static tension is 8.37 N (red line), and ideally the plot should be symmetrical about the red line. Effort has been made to mitigate this issue by increasing the voltage gain of signals and by improving the rigidity of the sensor connection. But these ended up with the same results.

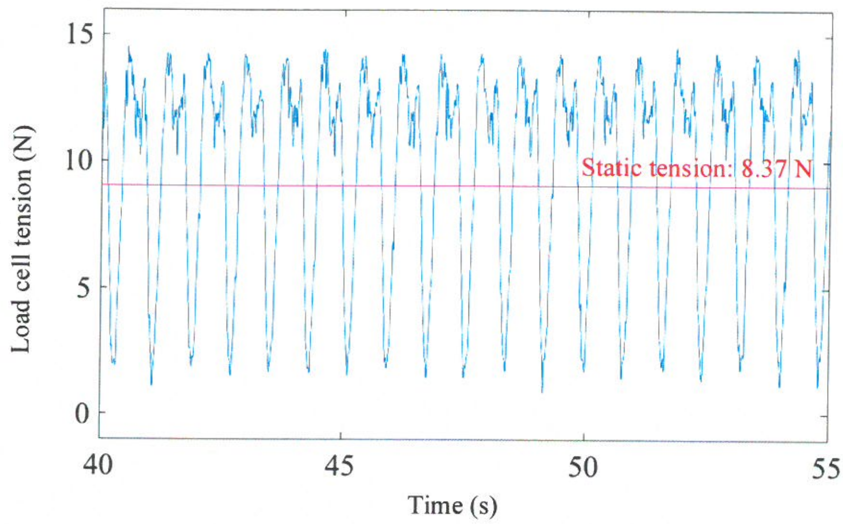


Figure 4.2.3 Time domain plot of load cell between 40 s and 55 s at 1.25 Hz applied frequency (experiment 2)

### 4.2.2 Accurate natural frequency by acceleration plots

Table 8.1 and Table 8.2 in the Appendix includes all the time domain and frequency domain responses of accelerations when the Perspex box floating system is in motion. The applied frequency range is between 0 to 2 Hz with the smallest increment being 0.01 Hz. The increments were adjusted such that the largest motion can be found to the most accurate frequency setting. There are some differences between the frequency set by the shaking table ('set frequency' in Table 8.1 and Table 8.2) and the frequency read from frequency domain MATLAB plots- frequency read from MATLAB seems more 'sticky'. Given that the acceleration changes when the 'set frequency' changes, this 'sticky' behaviour should not be a problem.

Figure 4.2.4 plots the maximum acceleration of MEM4 against all the 'set frequencies for the Perspex TLP system with 151 mm depth of water displaced (experiment 2). It can be seen from Table 8.1 that the largest acceleration is 3.501 $m/s^2$ at 1.25 Hz, and hence 1.25 Hz is the natural frequency (first mode of resonance). This was recorded with the frequency increment being 0.01 Hz which is the machine's limit.

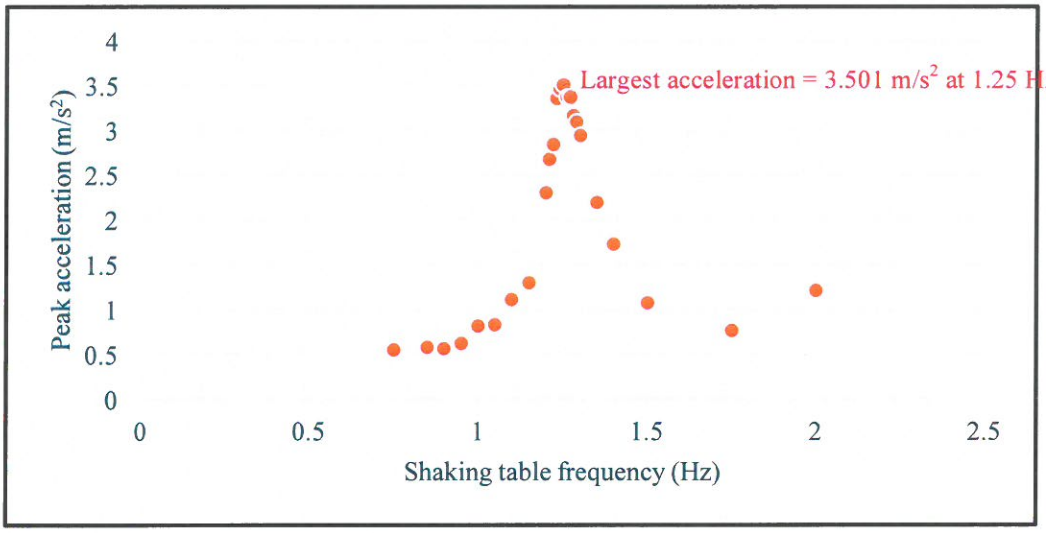


Figure 4.2.4 Maximum acceleration of MEM4 with respect to 'set frequency'
(experiment 2, depth of water displaced=151 mm, static tension in tendon=9.04 N)

Similarly, Figure 4.2.5 plots the maximum acceleration of MEM4 against all the frequencies for the system with 120 mm depth of water displaced (experiment 3). The largest acceleration is 3.822 $m/s^2$ at 1.21 Hz, and hence 1.21 Hz is the natural frequency (first mode of resonance) for 120 mm water depth.

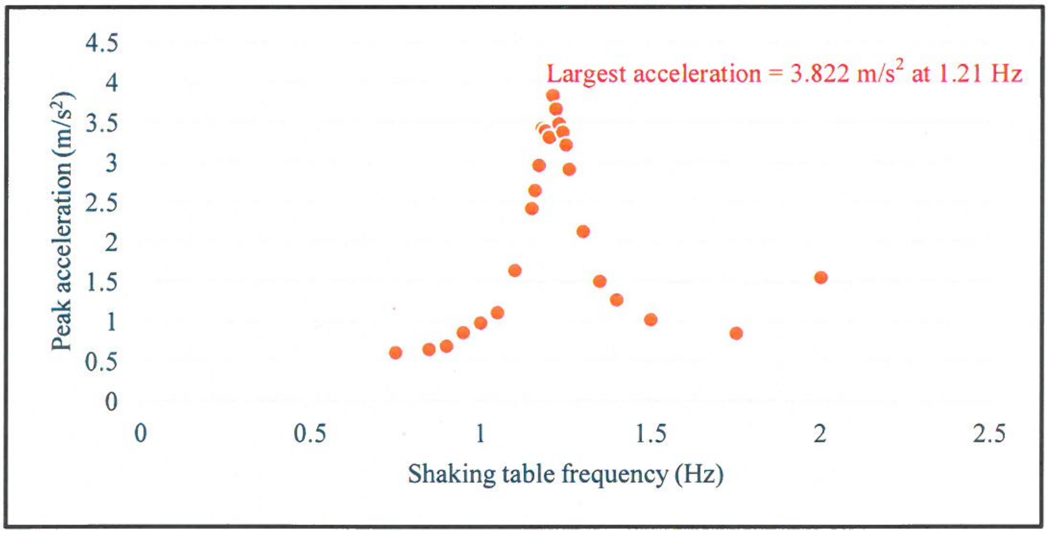


Figure 4.2.5 Maximum acceleration of MEM4 with respect to 'set frequency'
(experiment 3, depth of water displaced=120 mm, static tension in tendon=6.04 N)

In summary, at 151 mm, the largest acceleration is 3.501 $m/s^2$ at the natural frequency of 1.25 Hz; at 120 mm, the largest acceleration is 3.822 $m/s^2$ at the natural frequency of 1.21 Hz. It is obvious that when the water depth is smaller, the natural frequency is lower.

### 4.2.3 Accurate natural frequency by tension plots

Similar method can be used for the tension data. Table 8.3 and Table 8.4 in the Appendix includes all the time domain and frequency domain responses of tensions. Instead of using maximum values in Section 4.2.2, minimum values of the sinusoidal curves were adopted into the tables. This is because the load cell has some non-ideal behaviour due to compression of the connection (Figure 4.2.3)- the maximum values of these curves are no longer physically valid.

Figure 4.2.6 and 4.2.7 have been given to illustrate the minimum tension at different applied frequencies. It can be concluded that, from the tension point of view, the natural frequency is 1.27 Hz at 151 mm water depth and 1.16 Hz at 120 mm water depth. These are different from the natural frequency results (1.25 Hz and 1.21 Hz) obtained from the acceleration plots. The most likely cause is that the connection of the load cell is not rigid enough which resulted in the bad readings of the tensions. Therefore, it is less reliable to look at the minimum tension at different frequencies to conclude the natural frequency in these two experiment. But it is still true that a smaller water depth would yield a lower natural frequency.

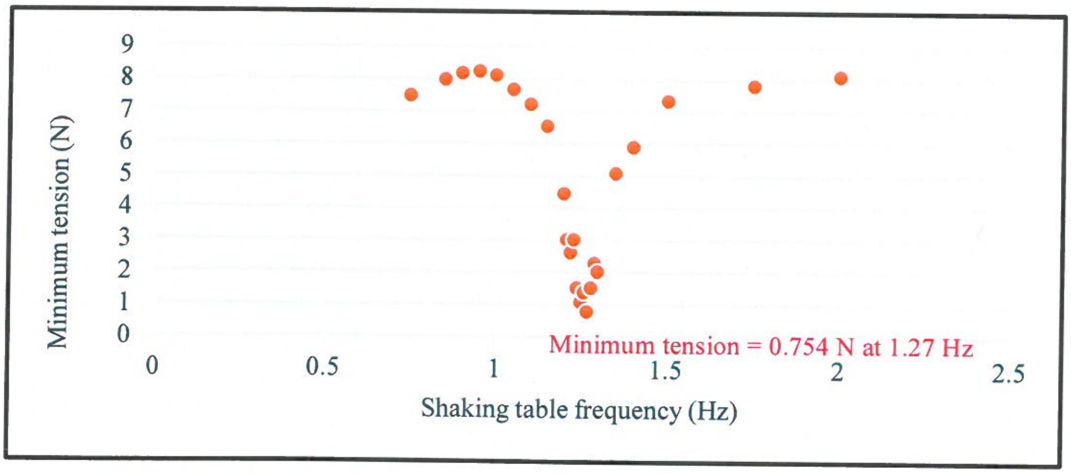


Figure 4.2.6 Minimum tensions of load cell with respect to 'set frequency' (experiment 2, depth of water displaced=151 mm, static tension in tendon=9.04 N)

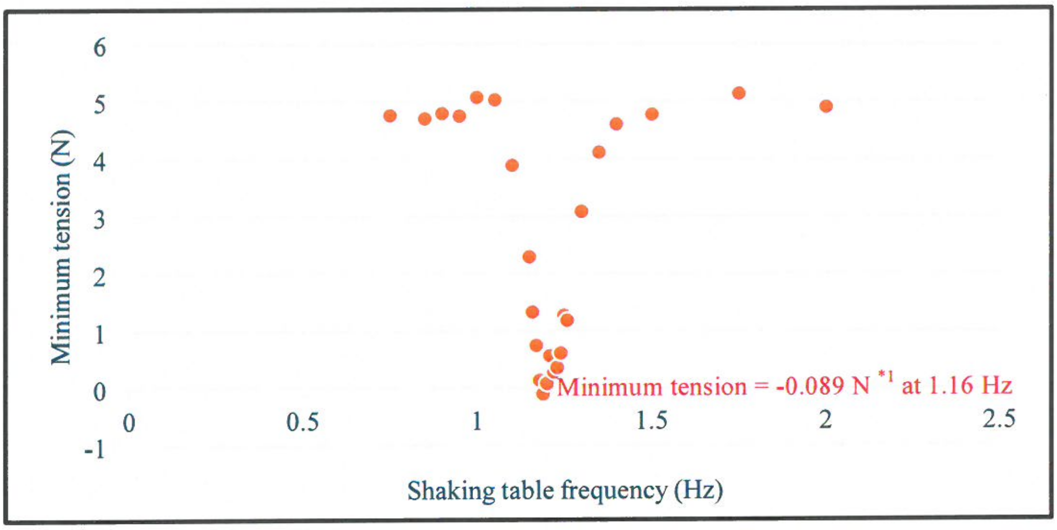


*1 It is impossible for a tension to be smaller than 0. This should be an experimental error. It may be due to the bad connection of the load cell.

Figure 4.2.7 Minimum tensions of load cell with respect to 'set frequency' (experiment 3, depth of water displaced=120 mm, static tension in tendon=6.04 N)

## 4.3 Replaced floating system with plate anchor foundations (experiment 4)

Figure 4.3.1 shows the experimental setup at the 180 mm embedment. The purpose of experiment 4 is mainly to investigate the depth of embedment such that the stability and strength would be sufficient. Therefore, several depths were chosen to compare the results. These include the initial depth of embedment 180 mm and two reduced depths 150 mm and 100 mm. The 180 mm test was performed first. Sand was then excavated to reduce the embedment.

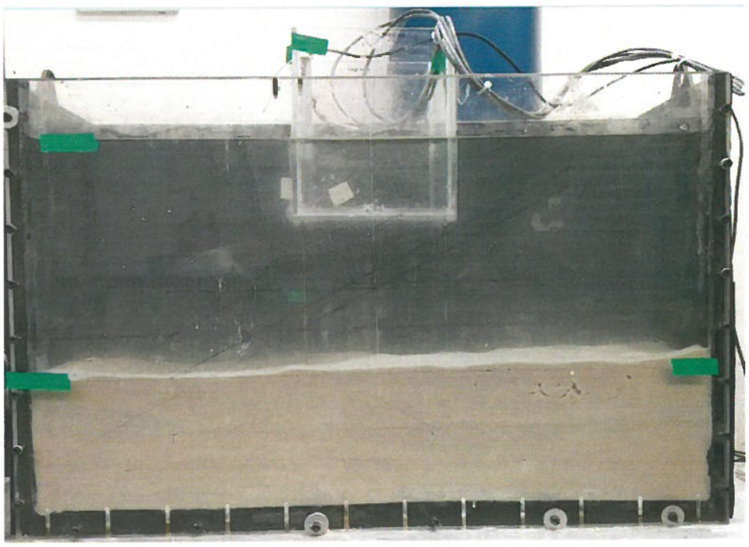

Figure 4.3.1 Experiment 4 setup with 180 mm embedment depth

As described in Table 3.3.2, the depth of embedment was determined to be 180 mm. This is an embedment depth with 1.54 factor of safety for 151 mm of water depth. However, the actual water depth was only 90 mm due to the size limitation of the water tank (static tension=3.787 N in one tendon). This resulted in a safety factor of 1.83 with 180 mm embedment (Eq. 3.3.3, with the tension T dynamically amplified by 3 times). This is a relatively high safety factor. Table 4.3.1 summarises the depth of embedment and their respective safety factors.

Table 4.3.1 Embedment depth and safety factor

| **Embedment depth (mm)** | 180 | 150 | 100 |
|---|---|---|---|
| **Safety factor** | 1.83 | 1.62 | 1.28 |

Again, frequencies from 0 to 2 Hz were applied at an increment of 0.25 Hz. The test of embedment was successful with embedment being 180 mm and 150 mm. The anchors were holding the TLP model firmly in place. Even at the largest acceleration, the anchor plate foundation was able to provide sufficient stability and strength.

At 100 mm of embedment, however, one of the anchors was displaced upwards after filling the water tank to the required depth. Although this embedment should yield a safety factor of 1.28, the anchor strength was not high enough to sustain the tension. There are several possibilities which may cause this failure:

- A bad sand pouring process. This would reduce the actual dry unit weight $\gamma'_s$ of sand.
- Disturbance of sand due to the excavation. This would also reduce $\gamma'_s$.
- Small displacement of anchors due to 180 mm and 150 mm tests. Although it was impossible to observe anchors underneath the sand, the anchors may have been moved during the first two tests. This will reduce the stability of the system.

# 5. Conclusions

## 5.1 Conclusions for experimental results

- The preliminary experiment has determined that sensors can be used to record parameters such as acceleration and tension of a physical TLP model. MATLAB is a convenient tool for applying digital filters, calibrating the voltages to physical terms and making appropriate plots.

- Key performance metrics for a TLP system are depth of water displaced by the floating system, weight of the system, tension within the mooring lines and depth of embedment for anchor foundations. By controlling specific variables, different experiments can be compared to conclude various results.

- There are limitations of the physical modelling method. The complexity of a scaled-down physical model can be high; it was hard to provide a fully simulated ocean wave with limited equipment; sensor problems such as the load cell problem in experiment 2 and 3 existed.

- Natural frequency can be found by applying different frequencies to the TLP system and by observing the frequency responses. Highly accurate natural frequency is possible to be found with minimal increment in frequency steps.

- Depth of embedment can be calculated and physically tested. A high factor of safety such as 1.8 is desirable due to the variability of the embedment sand density. For an actual design of foundation, in-situ soil data needs to be used to optimise the design.

## 5.2 Suggestions for future work

- It is possible to further improve the physical appearance of the floating system. Mass distribution can be considered such that it will simulate a wind turbine with high centre of gravity.

- The reliability of obtaining the tension needs to be improved. This may involve a different type of the load cell attachment.

- Noise recorded by sensors may be mitigated using more advanced method such as manipulating the gains of the sensors, applying better digital filters, etc.

- Embedment design can be refined to take into consideration of the cable factor. Currently no discussion has been made toward the resistance of mooring cable in sand- the upper part of the mooring cable in sand was observed to move rather than static.

- Anchor design can be improved. Plate anchors are not ideal as they do not utilise the friction between the anchor surface and sand to provide stability and strength.

## 6. Acknowledgements

Thanks to my supervisor, Prof. Gopal Madahbushi, for proposing this interesting project and helping me through all the difficulties I encountered over the last year; to Srikanth Madabhushi for guiding me to setup and calibrate the sensors; to Stefan Ritter for helping me with the MEMS sensor calibrations; to the technicians at the Schofield Centre: John Chandler, Tim Ablett, David Layfield, Chris McGinnie, Kristian Pether, Chris Knight, Mark Smith and Richard Adams, for their help with all the equipment needed.

## 7. References

[1] Arapogianni A and Genachte A, the members of the European Wind Energy Association's (EWEA) Offshore Wind Industry Group (OWIG), *Deep Water – The next step for offshore wind energy*, 2013

[2] Robertson A, Jonkman J.M., *Loads Analysis of Several Offshore Floating Wind Turbine Concepts*; Technical Report NREL/TP-5000-50539; National Renewable Energy Laboratory: Golden, CO, USA, 2011

[3] Suzuki K, Yamaguchi H, Akase M, Imakita A, Ishihara T, Fukumoto Y, Oyama T, *Initial design of tension leg platform for offshore wind farm*. J. Fluid Sci. Technol. 2011, 6, 372–381

[4] Bachynski EE, Moan T, *Design Considerations for Tension Leg Platform Wind Turbines*. Marine Structures. vol. 29., 2012

[5] Chandrasekaran S, *Dynamic Analysis and Design of Offshore Structures*. 2015, 25-61, ISBN: 978-81-322-2276-7

[6] Byrne BW, Houlsby GT. 2015 *Helical piles: an innovative foundation design option for o shore wind turbines*. Phil. Trans. R. Soc. A 373: 20140081

[7] Center for Wind Energy at James Madison University, *Review of Options for Offshore Foundation Substructures*, Aug. 2012

[8] Butterfield S, Jonkman J, and Musial W, National Renewable Energy Laboratory, *Coupled Dynamic Modeling of Floating Wind Turbine Systems*, 2006

[9] Casale C, Lembo E, Serri L, Viani S, *Preliminary Design of a Floating Wind Turbine Support Structure and Relevant System Cost Assessment*, CESI RICERCA S.p.A.

[10] Botta G, Lembo E, Serri L, Mazzocchi L, *Studio preliminare del comportamento dinamico di un aerogeneratore offshore su supporto galleggiante*, CESI RICERCA report, ref. No. 08000990, 2008

[11] Matha D, *Model Development and Loads Analysis of an Offshore Wind Turbine on a Tension Leg Platform with a Comparison to Other Floating Turbine Concepts*, Subcontract Report NREL/SR-500-45891, National Renewable Energy Laboratory, 2009

[12] Daniel E, *The Response of Floating Offshore Wind Farms*, Cambridge University Engineering Department, 2015

## 8. Appendix

Table 8.1 Frequency response chart for MEM4 acceleration with 151 mm depth of water displacement, experiment 2

| Set frequency (Hz) | Frequency read from frequency domain (Hz) | Peak acceleration in time domain ($m/s^2$) | Fourier amplitude in frequency domain ($m/s^2$) |
|---|---|---|---|
| 0.25 | (Values are too small to be read so neglected.) | | |
| 0.50 | | | |
| 0.75 | 0.733 | 0.542 | 0.358 |
| 0.85 | 0.800 | 0.572 | 0.307 |
| 0.90 | 0.867 | 0.561 | 0.387 |
| 0.95 | 0.933 | 0.615 | 0.466 |
| 1.00 | 1.000 | 0.806 | 0.390 |
| 1.05 | 1.000 | 0.827 | 0.575 |
| 1.10 | 1.067 | 1.105 | 0.898 |
| 1.15 | 1.133 | 1.289 | 1.233 |
| 1.20 | 1.200 | 2.297 | 1.538 |
| 1.21 | 1.200 | 2.667 | 2.196 |
| 1.22 | 1.200 | 2.836 | 2.664 |
| 1.23 | 1.200 | 3.354 | 2.986 |
| 1.24 | 1.200 | 3.458 | 3.110 |
| 1.25 | 1.200 | 3.501 | 2.910 |
| 1.26 | 1.200 | 3.367 | 2.436 |
| 1.27 | 1.267 | 3.364 | 2.488 |
| 1.28 | 1.267 | 3.159 | 2.979 |
| 1.29 | 1.267 | 3.084 | 3.123 |
| 1.30 | 1.267 | 2.932 | 3.004 |
| 1.35 | 1.333 | 2.186 | 1.979 |
| 1.40 | 1.400 | 1.718 | 1.043 |
| 1.50 | 1.467 | 1.064 | 0.960 |
| 1.75 | 1.733 | 0.758 | 0.528 |
| 2.00 | 1.933 | 1.205 | 0.902 |

Table 8.2 Frequency response chart for MEM4 acceleration with 120 mm depth of water displacement, experiment 3

| Set frequency (Hz) | Frequency read from frequency domain (Hz) | Peak acceleration in time domain ($m/s^2$) | Fourier amplitude in frequency domain ($m/s^2$) |
|---|---|---|---|
| 0.25 | (Values are too small to be read so neglected.) | | |
| 0.50 | | | |
| 0.75 | 0.733 | 0.600 | 0.3994 |
| 0.85 | 0.800 | 0.641 | 0.2857 |
| 0.90 | 0.867 | 0.678 | 0.4692 |
| 0.95 | 0.933 | 0.851 | 0.5963 |
| 1.00 | 1.000 | 0.974 | 0.6752 |
| 1.05 | 1.000 | 1.097 | 0.7909 |
| 1.10 | 1.067 | 1.630 | 1.418 |
| 1.15 | 1.133 | 2.411 | 2.402 |
| 1.16 | 1.133 | 2.632 | 2.676 |
| 1.17 | 1.133 | 2.947 | 2.907 |
| 1.18 | 1.133 | 3.417 | 2.88 |
| 1.19 | 1.133 | 3.382 | 2.503 |
| 1.20 | 1.200 | 3.301 | 2.53 |
| 1.21 | 1.200 | 3.822 | 3.169 |
| 1.22 | 1.200 | 3.657 | 3.352 |
| 1.23 | 1.200 | 3.473 | 3.242 |
| 1.24 | 1.200 | 3.367 | 3.036 |
| 1.25 | 1.200 | 3.203 | 2.519 |
| 1.26 | 1.200 | 2.897 | 1.841 |
| 1.30 | 1.267 | 2.122 | 2.046 |
| 1.35 | 1.333 | 1.496 | 1.409 |
| 1.40 | 1.400 | 1.263 | 0.8625 |
| 1.50 | 1.467 | 1.011 | 0.8478 |
| 1.75 | 1.733 | 0.838 | 0.5723 |
| 2.00 | 1.933 | 1.539 | 1.279 |

Table 8.3 Frequency response chart for tensions with 151 mm depth of water displacement, experiment 2

| Set frequency (Hz) | Frequency read from frequency domain (Hz) | Min. tension in time domain (N) | Fourier amplitude in frequency domain (N) |
|---|---|---|---|
| 0.25 | (Values are too small to be read so neglected.) | | |
| 0.50 | | | |
| 0.75 | 0.720 | 7.448 | 1.153 |
| 0.85 | 0.840 | 7.946 | 0.758 |
| 0.90 | 0.880 | 8.154 | 1.084 |
| 0.95 | 0.920 | 8.204 | 1.019 |
| 1.00 | 0.960 | 8.093 | 1.049 |
| 1.05 | 1.040 | 7.644 | 0.915 |
| 1.10 | 1.080 | 7.196 | 1.758 |
| 1.15 | 1.120 | 6.511 | 2.107 |
| 1.20 | 1.160 | 4.421 | 2.980 |
| 1.21 | 1.200 | 2.984 | 2.563 |
| 1.22 | 1.200 | 2.599 | 3.844 |
| 1.23 | 1.200 | 2.992 | 4.426 |
| 1.24 | 1.200 | 1.501 | 4.247 |
| 1.25 | 1.200 | 1.055 | 3.336 |
| 1.26 | 1.240 | 1.353 | 4.388 |
| 1.27 | 1.240 | 0.754 | 4.864 |
| 1.28 | 1.240 | 1.504 | 4.340 |
| 1.29 | 1.240 | 2.249 | 3.038 |
| 1.30 | 1.280 | 1.997 | 3.946 |
| 1.35 | 1.320 | 5.059 | 2.966 |
| 1.40 | 1.360 | 5.868 | 1.840 |
| 1.50 | 1.480 | 7.301 | 1.134 |
| 1.75 | 1.720 | 7.788 | 0.808 |
| 2.00 | 1.960 | 8.090 | 0.645 |

Table 8.4 Frequency response chart for tensions with 120 mm depth of water displacement, experiment 3

| Set frequency (Hz) | Frequency read from frequency domain (Hz) | Min. tension in time domain (N) | Fourier amplitude in frequency domain (N) |
|---|---|---|---|
| 0.25 | (Values are too small to be read so neglected.) | | |
| 0.50 | | | |
| 0.75 | 0.720 | 4.758 | 0.4392 |
| 0.85 | 0.840 | 4.710 | 0.3793 |
| 0.90 | 0.880 | 4.794 | 0.395 |
| 0.95 | 0.960 | 4.754 | 0.3309 |
| 1.00 | 1.000 | 5.076 | 0.3965 |
| 1.05 | 1.040 | 5.031 | 0.5248 |
| 1.10 | 1.080 | 3.886 | 1.117 |
| 1.15 | 1.120 | 2.292 | 2.163 |
| 1.16 | 1.120 | 1.328 | 2.129 |
| 1.17 | 1.160 | 0.755 | 2.144 |
| 1.18 | 1.160 | 0.144 | 2.939 |
| 1.19 | 1.160 | -0.089 | 3.303 |
| 1.20 | 1.160 | 0.088 | 3.046 |
| 1.21 | 1.200 | 0.575 | 2.55 |
| 1.22 | 1.200 | 0.292 | 3.003 |
| 1.23 | 1.200 | 0.370 | 2.988 |
| 1.24 | 1.200 | 0.610 | 2.5 |
| 1.25 | 1.240 | 1.278 | 1.927 |
| 1.26 | 1.240 | 1.187 | 2.323 |
| 1.30 | 1.280 | 3.086 | 1.45 |
| 1.35 | 1.320 | 4.113 | 1.026 |
| 1.40 | 1.360 | 4.610 | 0.6345 |
| 1.50 | 1.480 | 4.777 | 0.5407 |
| 1.75 | 1.720 | 5.130 | 0.3618 |
| 2.00 | 1.960 | 4.900 | 0.3988 |

## 9. Retrospective risk assessment

The health and safety aspect of this project was overall good. With an early risk assessment, most of the risks were mitigated. The main hazards were from mechanical hazard, weight lifting hazard and electrical hazard.

**Mechanical hazard**

The main source of mechanical hazard comes from the shaking table. It includes the driving motor, driving chain and the moving water tank. A special acrylic enclosure was used to cover all the driving parts of the shaking table. A useful lid was designed such that if it was not closed, the motor would not start rotating. Before each test was started, an inspection of the surrounding of the shaking table was done to make sure there was nothing obstructing the movement of the shaking table. Test runs were also done such that water leakages can be mitigated as early as possible.

**Electrical hazard**

Electrical hazard is mainly from the shaking table driving circuit and the data logger (a desktop PC). All the cables were examined for bad shielding and bad connection. The electrical connectors were placed far from any liquid and were raised high enough to prevent any ground level flood. Unnecessary electrical appliances are always switched off with mains sockets unplugged. Cable management was done such that the mechanical moving parts will not interfere with any cables and trip hazard is minimised.

**Weight lifting hazard**

In this project, there was a need to perform weight lifting for the sand pouring process. A crane was used to lift the funnel containing sand to do the pouring. Manual weight lifting was limited to an acceptable weight such that the person would not feel uncomfortable. Gloves with grip were worn whenever possible to reduce the chance of slip.

With progressively familiar use of all the equipment, the self-awareness of safety has also grown. Overall, the safety was successfully ensured for this project.